The MEMS Handbook

Second Edition

MEMS

Introduction and Fundamentals

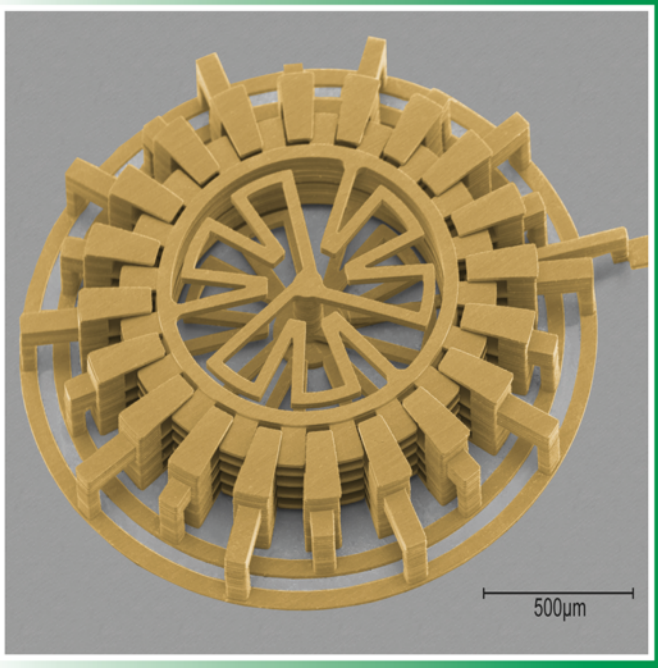

Edited by
Mohamed Gad-el-Hak

CRC Taylor & Francis
Taylor & Francis Group

The MEMS Handbook Second Edition

MEMS

Introduction and Fundamentals

Mechanical Engineering Series

Frank Kreith and Roop Mahajan - Series Editors

Published Titles

Distributed Generation: The Power Paradigm for the New Millennium
Anne-Marie Borbely & Jan F. Kreider
Elastoplasticity Theory
Vlado A. Lubarda
Energy Audit of Building Systems: An Engineering Approach
Moncef Krarti
Engineering Experimentation
Euan Somerscales
Entropy Generation Minimization
Adrian Bejan
Finite Element Method Using MATLAB, 2nd Edition
Young W. Kwon & Hyochoong Bang
Fluid Power Circuits and Controls: Fundamentals and Applications
John S. Cundiff
Fundamentals of Environmental Discharge Modeling
Lorin R. Davis
Heat Transfer in Single and Multiphase Systems
Greg F. Naterer
Introductory Finite Element Method
Chandrakant S. Desai & Tribikram Kundu
Intelligent Transportation Systems: New Principles and Architectures
Sumit Ghosh & Tony Lee
Mathematical & Physical Modeling of Materials Processing Operations
Olusegun Johnson Ilegbusi, Manabu Iguchi & Walter E. Wahnsiedler
Mechanics of Composite Materials
Autar K. Kaw
Mechanics of Fatigue
Vladimir V. Bolotin
Mechanics of Solids and Shells: Theories and Approximations
Gerald Wempner & Demosthenes Talaslidis
Mechanism Design: Enumeration of Kinematic Structures According to Function
Lung-Wen Tsai
The MEMS Handbook, Second Edition
MEMS: Introduction and Fundamentals
MEMS: Design and Fabrication
MEMS: Applications
Mohamed Gad-el-Hak
Nonlinear Analysis of Structures
M. Sathyamoorthy
Practical Inverse Analysis in Engineering
David M. Trujillo & Henry R. Busby
Pressure Vessels: Design and Practice
Somnath Chattopadhyay
Principles of Solid Mechanics
Rowland Richards, Jr.
Thermodynamics for Engineers
Kau-Fui Wong
Vibration and Shock Handbook
Clarence W. de Silva
Viscoelastic Solids
Roderic S. Lakes

The MEMS Handbook Second Edition

MEMS

Introduction and Fundamentals

Edited by
Mohamed Gad-el-Hak

Taylor & Francis
Taylor & Francis Group
Boca Raton London New York

A CRC title, part of the Taylor & Francis imprint, a member of the Taylor & Francis Group, the academic division of T&F Informa plc.

Foreground: A 24-layer rotary varactor fabricated in nickel using the Electrochemical Fabrication (EFAB®) technology. See Chapter 6, *MEMS: Design and Fabrication*, for details of the EFAB® technology. Scanning electron micrograph courtesy of Adam L. Cohen, Microfabrica Incorporated (www.microfabrica.com), U.S.A.

Background: A two-layer surface macromachined, vibrating gyroscope. The overall size of the integrated circuitry is 4.5 × 4.5 mm. Sandia National Laboratories' emblem in the lower right-hand corner is 700 microns wide. The four silver rectangles in the center are the gyroscope's proof masses, each 240 × 310 × 2.25 microns. See Chapter 4, *MEMS: Applications* (0-8493-9139-3), for design and fabrication details. Photograph courtesy of Andrew D. Oliver, Sandia National Laboratories.

Published in 2006 by
CRC Press
Taylor & Francis Group
6000 Broken Sound Parkway NW, Suite 300
Boca Raton, FL 33487-2742

Printed in the United States of America on acid-free paper
10 9 8 7 6 5 4 3 2 1

International Standard Book Number-10: 0-8493-9137-7 (Hardcover)
International Standard Book Number-13: 978-0-8493-9137-8 (Hardcover)
Library of Congress Card Number 2005050111

Library of Congress Cataloging-in-Publication Data

MEMS : introduction and fundamentals / edited by Mohamed Gad-El-Hak.
p. cm. -- (Mechanical engineering series)
Includes bibliographical references and index.
ISBN 0-8493-9137-7 (alk. paper)
1. Microelectronics. 2. Nanotechnology. I. Gad-el-Hak, M. II. Mechanical engineering series (Boca Raton, Fla.)

TK7874.M3762 2005
621.381--dc22 2005050111

informa
Taylor & Francis Group
is the Academic Division of Informa plc.

Visit the Taylor & Francis Web site at
http://www.taylorandfrancis.com

and the CRC Press Web site at
http://www.crcpress.com

Preface

In a little time I felt something alive moving on my left leg, which advancing gently forward over my breast, came almost up to my chin; when bending my eyes downward as much as I could, I perceived it to be a human creature not six inches high, with a bow and arrow in his hands, and a quiver at his back. … I had the fortune to break the strings, and wrench out the pegs that fastened my left arm to the ground; for, by lifting it up to my face, I discovered the methods they had taken to bind me, and at the same time with a violent pull, which gave me excessive pain, I a little loosened the strings that tied down my hair on the left side, so that I was just able to turn my head about two inches. … These people are most excellent mathematicians, and arrived to a great perfection in mechanics by the countenance and encouragement of the emperor, who is a renowned patron of learning. This prince has several machines fixed on wheels, for the carriage of trees and other great weights.

(**From *Gulliver's Travels—A Voyage to Lilliput*, by Jonathan Swift, 1726.**)

In the Nevada desert, an experiment has gone horribly wrong. A cloud of nanoparticles — micro-robots — has escaped from the laboratory. This cloud is self-sustaining and self-reproducing. It is intelligent and learns from experience. For all practical purposes, it is alive.

It has been programmed as a predator. It is evolving swiftly, becoming more deadly with each passing hour.

Every attempt to destroy it has failed.

And we are the prey.

(**From Michael Crichton's techno-thriller *Prey*, HarperCollins Publishers, 2002.**)

Almost three centuries apart, the imaginative novelists quoted above contemplated the astonishing, at times frightening possibilities of living beings much bigger or much smaller than us. In 1959, the physicist Richard Feynman envisioned the fabrication of machines much smaller than their makers. The length scale of man, at slightly more than 10^0 m, amazingly fits right in the middle of the smallest subatomic particle, which is approximately 10^{-26} m, and the extent of the observable universe, which is of the order of 10^{26} m. Toolmaking has always differentiated our species from all others on Earth. Close to 400,000 years ago, archaic *Homo sapiens* carved aerodynamically correct wooden spears. Man builds things consistent with his size, typically in the range of two orders of magnitude larger or smaller than himself. But humans have always striven to explore, build, and control the extremes of length and time scales. In the voyages to Lilliput and Brobdingnag in *Gulliver's Travels*, Jonathan Swift speculates on the remarkable possibilities which diminution or magnification of physical dimensions provides. The Great Pyramid of Khufu was originally 147 m high when completed around 2600 B.C., while the Empire State Building constructed in 1931 is presently 449 m high. At the other end of the spectrum of manmade artifacts, a dime is slightly less than 2 cm in diameter. Watchmakers have practiced the art of miniaturization since the 13th century. The invention of the microscope in the 17th century opened the way for direct observation of microbes and plant and animal cells. Smaller things were

manmade in the latter half of the 20th century. The transistor in today's integrated circuits has a size of 0.18 micron in production and approaches 10 nanometers in research laboratories.

Microelectromechanical systems (MEMS) refer to devices that have characteristic length of less than 1 mm but more than 1 micron, that combine electrical and mechanical components, and that are fabricated using integrated circuit batch-processing technologies. Current manufacturing techniques for MEMS include surface silicon micromachining; bulk silicon micromachining; lithography, electrodeposition, and plastic molding; and electrodischarge machining. The multidisciplinary field has witnessed explosive growth during the last decade and the technology is progressing at a rate that far exceeds that of our understanding of the physics involved. Electrostatic, magnetic, electromagnetic, pneumatic and thermal actuators, motors, valves, gears, cantilevers, diaphragms, and tweezers of less than 100 micron size have been fabricated. These have been used as sensors for pressure, temperature, mass flow, velocity, sound and chemical composition, as actuators for linear and angular motions, and as simple components for complex systems such as robots, lab-on-a-chip, micro heat engines and micro heat pumps. The lab-on-a-chip in particular is promising to automate biology and chemistry to the same extent the integrated circuit has allowed large-scale automation of computation. Global funding for micro- and nanotechnology research and development quintupled from $432 million in 1997 to $2.2 billion in 2002. In 2004, the U.S. National Nanotechnology Initiative had a budget of close to $1 billion, and the worldwide investment in nanotechnology exceeded $3.5 billion. In 10 to 15 years, it is estimated that micro- and nanotechnology markets will represent $340 billion per year in materials, $300 billion per year in electronics, and $180 billion per year in pharmaceuticals.

The three-book *MEMS set* covers several aspects of microelectromechanical systems, or more broadly, the art and science of electromechanical miniaturization. MEMS design, fabrication, and application as well as the physical modeling of their materials, transport phenomena, and operations are all discussed. Chapters on the electrical, structural, fluidic, transport and control aspects of MEMS are included in the books. Other chapters cover existing and potential applications of microdevices in a variety of fields, including instrumentation and distributed control. Up-to-date new chapters in the areas of microscale hydrodynamics, lattice Boltzmann simulations, polymeric-based sensors and actuators, diagnostic tools, microactuators, nonlinear electrokinetic devices, and molecular self-assembly are included in the three books constituting the second edition of *The MEMS Handbook*. The 16 chapters in *MEMS: Introduction and Fundamentals* provide background and physical considerations, the 14 chapters in *MEMS: Design and Fabrication* discuss the design and fabrication of microdevices, and the 15 chapters in *MEMS: Applications* review some of the applications of micro-sensors and microactuators.

There are a total of 45 chapters written by the world's foremost authorities in this multidisciplinary subject. The 71 contributing authors come from Canada, China (Hong Kong), India, Israel, Italy, Korea, Sweden, Taiwan, and the United States, and are affiliated with academia, government, and industry. Without compromising rigorousness, the present text is designed for maximum readability by a broad audience having engineering or science background. As expected when several authors are involved, and despite the editor's best effort, the chapters of each book vary in length, depth, breadth, and writing style. These books should be useful as references to scientists and engineers already experienced in the field or as primers to researchers and graduate students just getting started in the art and science of electromechanical miniaturization. The Editor-in-Chief is very grateful to all the contributing authors for their dedication to this endeavor and selfless, generous giving of their time with no material reward other than the knowledge that their hard work may one day make the difference in someone else's life. The talent, enthusiasm, and indefatigability of Taylor & Francis Group's Cindy Renee Carelli (acquisition editor), Jessica Vakili (production coordinator), N. S. Pandian and the rest of the editorial team at Macmillan India Limited, Mimi Williams and Tao Woolfe (project editors) were highly contagious and percolated throughout the entire endeavor.

Mohamed Gad-el-Hak

Editor-in-Chief

Mohamed Gad-el-Hak received his B.Sc. (summa cum laude) in mechanical engineering from Ain Shams University in 1966 and his Ph.D. in fluid mechanics from the Johns Hopkins University in 1973, where he worked with Professor Stanley Corrsin. Gad-el-Hak has since taught and conducted research at the University of Southern California, University of Virginia, University of Notre Dame, Institut National Polytechnique de Grenoble, Université de Poitiers, Friedrich-Alexander-Universität Erlangen-Nürnberg, Technische Universität München, and Technische Universität Berlin, and has lectured extensively at seminars in the United States and overseas. Dr. Gad-el-Hak is currently the Inez Caudill Eminent Professor of Biomedical Engineering and chair of mechanical engineering at Virginia Commonwealth University in Richmond. Prior to his Notre Dame appointment as professor of aerospace and mechanical engineering, Gad-el-Hak was senior research scientist and program manager at Flow Research Company in Seattle, Washington, where he managed a variety of aerodynamic and hydrodynamic research projects.

Professor Gad-el-Hak is world renowned for advancing several novel diagnostic tools for turbulent flows, including the laser-induced fluorescence (LIF) technique for flow visualization; for discovering the efficient mechanism via which a turbulent region rapidly grows by destabilizing a surrounding laminar flow; for conducting the seminal experiments which detailed the fluid–compliant surface interactions in turbulent boundary layers; for introducing the concept of targeted control to achieve drag reduction, lift enhancement and mixing augmentation in wall-bounded flows; and for developing a novel viscous pump suited for microelectromechanical systems (MEMS) applications. Gad-el-Hak's work on Reynolds number effects in turbulent boundary layers, published in 1994, marked a significant paradigm shift in the subject. His 1999 paper on the fluid mechanics of microdevices established the fledgling field on firm physical grounds and is one of the most cited articles of the 1990s.

Gad-el-Hak holds two patents: one for a drag-reducing method for airplanes and underwater vehicles and the other for a lift-control device for delta wings. Dr. Gad-el-Hak has published over 450 articles, authored/edited 14 books and conference proceedings, and presented 250 invited lectures in the basic and applied research areas of isotropic turbulence, boundary layer flows, stratified flows, fluid–structure interactions, compliant coatings, unsteady aerodynamics, biological flows, non-Newtonian fluids, hard and soft computing including genetic algorithms, flow control, and microelectromechanical systems. Gad-el-Hak's papers have been cited well over 1000 times in the technical literature. He is the author of the book "*Flow Control: Passive, Active, and Reactive Flow Management*," and editor of the books "*Frontiers in Experimental Fluid Mechanics,*" "*Advances in Fluid Mechanics Measurements*," "*Flow Control: Fundamentals and Practices*," "*The MEMS Handbook,*" and "*Transition and Turbulence Control.*"

Professor Gad-el-Hak is a fellow of the American Academy of Mechanics, a fellow and life member of the American Physical Society, a fellow of the American Society of Mechanical Engineers, an associate fellow of the American Institute of Aeronautics and Astronautics, and a member of the European Mechanics

Society. He has recently been inducted as an eminent engineer in Tau Beta Pi, an honorary member in Sigma Gamma Tau and Pi Tau Sigma, and a member-at-large in Sigma Xi. From 1988 to 1991, Dr. Gad-el-Hak served as Associate Editor for *AIAA Journal*. He is currently serving as Editor-in-Chief for *e-MicroNano.com*, Associate Editor for *Applied Mechanics Reviews* and *e-Fluids*, as well as Contributing Editor for Springer-Verlag's *Lecture Notes in Engineering* and *Lecture Notes in Physics*, for McGraw-Hill's Year Book of Science and Technology, and for CRC Press' *Mechanical Engineering Series*.

Dr. Gad-el-Hak serves as consultant to the governments of Egypt, France, Germany, Italy, Poland, Singapore, Sweden, United Kingdom and the United States, the United Nations, and numerous industrial organizations. Professor Gad-el-Hak has been a member of several advisory panels for DOD, DOE, NASA and NSF. During the 1991/1992 academic year, he was a visiting professor at Institut de Mécanique de Grenoble, France. During the summers of 1993, 1994 and 1997, Dr. Gad-el-Hak was, respectively, a distinguished faculty fellow at Naval Undersea Warfare Center, Newport, Rhode Island, a visiting exceptional professor at Université de Poitiers, France, and a Gastwissenschaftler (guest scientist) at Forschungszentrum Rossendorf, Dresden, Germany. In 1998, Professor Gad-el-Hak was named the Fourteenth ASME Freeman Scholar. In 1999, Gad-el-Hak was awarded the prestigious Alexander von Humboldt Prize — Germany's highest research award for senior U.S. scientists and scholars in all disciplines — as well as the Japanese Government Research Award for Foreign Scholars. In 2002, Gad-el-Hak was named ASME Distinguished Lecturer, as well as inducted into the Johns Hopkins University Society of Scholars.

Contributors

Ronald J. Adrian
Department of Mechanical and Aerospace Engineering
Arizona State University
Tempe, Arizona, U.S.A.

Ramesh K. Agarwal
Department of Mechanical and Aerospace Engineering
Washington University in St. Louis
St. Louis, Missouri, U.S.A.

Ali Beskok
Department of Mechanical Engineering
Texas A&M University
College Station, Texas, U.S.A.

Thomas R. Bewley
Department of Mechanical and Aerospace Engineering
University of California, San Diego
La Jolla, California, U.S.A.

Kenneth S. Breuer
Division of Engineering
Brown University
Providence, Rhode Island, U.S.A.

Hsueh-Chia Chang
Center for Microfluidics and Medical Diagnostics
University of Notre Dame
Notre Dame, Indiana, U.S.A.

Mohamed Gad-el-Hak
Department of Mechanical Engineering
Virginia Commonwealth University
Richmond, Virginia, U.S.A.

J. William Goodwine
Department of Aerospace and Mechanical Engineering
University of Notre Dame
Notre Dame, Indiana, U.S.A.

Nicolas G. Hadjiconstantinou
Department of Mechanical Engineering
Massachusetts Institute of Technology
Cambridge, Massachusetts, U.S.A.

George Em Karniadakis
Center for Fluid Mechanics
Brown University
Providence, Rhode Island, U.S.A.

Robert M. Kirby
School of Computing
University of Utah
Salt Lake City, Utah, U.S.A.

Kartikeya Mayaram
Department of Electrical and Computer Engineering
Oregon State University
Corvallis, Oregon, U.S.A.

Oleg Mikulchenko
Advanced Mixed Signal Development
Intel Corporation
Sacramento, California, U.S.A.

Joshua I. Molho
Caliper Life Sciences Incorporated
Mountain View, California, U.S.A.

Alexander Oron
Department of Mechanical Engineering
Technion—Israel Institute of Technology
Haifa, Israel

Juan G. Santiago
Department of Mechanical Engineering
Stanford University
Stanford, California, U.S.A.

Mihir Sen
Department of Aerospace and Mechanical Engineering
University of Notre Dame
Notre Dame, Indiana, U.S.A.

Kendra V. Sharp
Department of Mechanical and Nuclear Engineering
Pennsylvania State University
University Park, Pennsylvania, U.S.A.

William N. Sharpe, Jr.
Department of Mechanical Engineering
The Johns Hopkins University
Baltimore, Maryland, U.S.A.

Robert H. Stroud
The Aerospace Corporation
Sterling, Virginia, U.S.A.

William Trimmer
Belle Mead Research, Inc.
Hillsborough, New Jersey, U.S.A.

Keon-Young Yun
Research & Development Center
Samhongsa Co., Ltd.
Seoul, Korea

Table of Contents

Preface v

Editor-in-Chief vii

Contributors ix

1 Introduction *Mohamed Gad-el-Hak* **1**-1

2 Scaling of Micromechanical Devices *William Trimmer and Robert H. Stroud* **2**-1

3 Mechanical Properties of MEMS Materials *William N. Sharpe, Jr.* **3**-1

4 Flow Physics *Mohamed Gad-el-Hak* **4**-1

5 Integrated Simulation for MEMS: Coupling Flow-Structure-Thermal-Electrical Domains *Robert M. Kirby, George Em Karniadakis, Oleg Mikulchenko and Kartikeya Mayaram* **5**-1

6 Molecular-Based Microfluidic Simulation Models *Ali Beskok* **6**-1

7 Hydrodynamics of Small-Scale Internal Gaseous Flows *Nicolas G. Hadjiconstantinou* **7**-1

8 Burnett Simulations of Flows in Microdevices *Ramesh K. Agarwal and Keon-Young Yun* **8**-1

9 Lattice Boltzmann Simulations of Slip Flow in Microchannels *Ramesh K. Agarwal* **9**-1

10 Liquid Flows in Microchannels *Kendra V. Sharp, Ronald J. Adrian, Juan G. Santiago and Joshua I. Molho* **10**-1

11 Lubrication in MEMS *Kenneth S. Breuer* **11**-1

12 Physics of Thin Liquid Films *Alexander Oron* **12**-1

13 Bubble/Drop Transport in Microchannels *Hsueh-Chia Chang* **13**-1

14 Fundamentals of Control Theory *J. William Goodwine* **14**-1

15 Model-Based Flow Control for Distributed Architectures
Thomas R. Bewley **15**-1

16 Soft Computing in Control *Mihir Sen and J. William Goodwine* **16**-1

Index **I**-1

The farther backward you can look,
the farther forward you are likely to see.

(Sir Winston Leonard Spencer Churchill, 1874–1965)

Janus, Roman god of gates, doorways and all beginnings, gazing both forward and backward.

As for the future, your task is not to foresee, but to enable it.

(Antoine-Marie-Roger de Saint-Exupéry, 1900–1944,
in Citadelle [*The Wisdom of the Sands*])

1

Introduction

Mohamed Gad-el-Hak
Virginia Commonwealth University

How many times when you are working on something frustratingly tiny, like your wife's wrist watch, have you said to yourself, "If I could only train an ant to do this!" What I would like to suggest is the possibility of training an ant to train a mite to do this. What are the possibilities of small but movable machines? They may or may not be useful, but they surely would be fun to make.

(From the talk "There's Plenty of Room at the Bottom," delivered by Richard P. Feynman at the annual meeting of the American Physical Society, Pasadena, California, December 1959.)

Toolmaking has always differentiated our species from all others on Earth. Aerodynamically correct wooden spears were carved by archaic *Homo sapiens* close to 400,000 years ago. Man builds things consistent with his size, typically in the range of two orders of magnitude larger or smaller than himself, as indicated in Figure 1.1. Though the extremes of length-scale are outside the range of this figure, man, at slightly more than 10^0 m, amazingly fits right in the middle of the smallest subatomic particle, which is

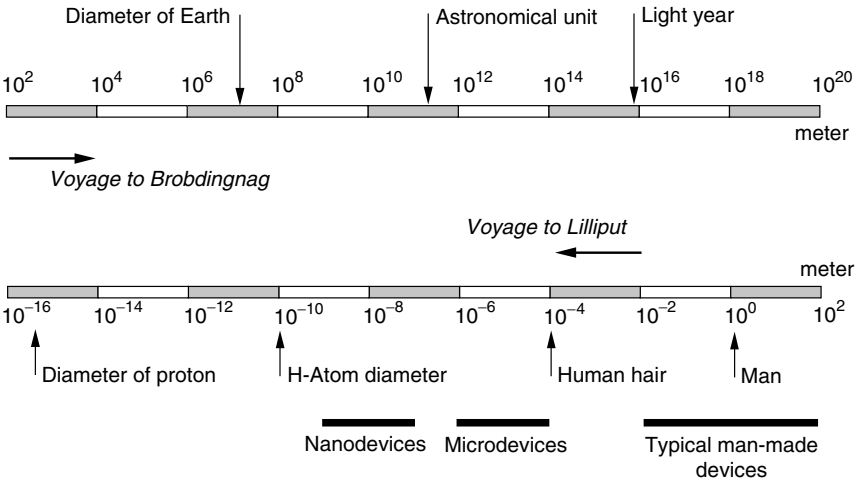

FIGURE 1.1 Scale of things, in meters. Lower scale continues in the upper bar from left to right. One meter is 10^6 microns, 10^9 nanometers, or 10^{10} Angstroms.

approximately 10^{-26} m, and the extent of the observable universe, which is of the order of 10^{26} m (15 billion light years); neither geocentric nor heliocentric, but rather egocentric universe. But humans have always striven to explore, build, and control the extremes of length and time scales. In the voyages to Lilliput and Brobdingnag of *Gulliver's Travels*, Jonathan Swift (1726) speculates on the remarkable possibilities which diminution or magnification of physical dimensions provides.[1] The Great Pyramid of Khufu was originally 147 m high when completed around 2600 B.C., while the Empire State Building constructed in 1931 is presently — after the addition of a television antenna mast in 1950 — 449 m high. At the other end of the spectrum of manmade artifacts, a dime is slightly less than 2 cm in diameter. Watchmakers have practiced the art of miniaturization since the 13th century. The invention of the microscope in the 17th century opened the way for direct observation of microbes and plant and animal cells. Smaller things were manmade in the latter half of the 20th century. The transistor — invented in 1947 — in today's integrated circuits has a size[2] of 0.18 micron (180 nanometers) in production and approaches 10 nm in research laboratories using electron beams. But what about the miniaturization of mechanical parts — machines — envisioned by Feynman (1961) in his legendary speech quoted above?

Manufacturing processes that can create extremely small machines have been developed in recent years (Angell et al., 1983; Gabriel et al., 1988, 1992; O'Connor, 1992; Gravesen et al., 1993; Bryzek et al., 1994; Gabriel, 1995; Ashley, 1996; Ho and Tai, 1996, 1998; Hogan, 1996; Ouellette, 1996, 2003; Paula, 1996; Robinson et al., 1996a, 1996b; Tien, 1997; Amato, 1998; Busch-Vishniac, 1998; Kovacs, 1998; Knight, 1999; Epstein, 2000; O'Connor and Hutchinson, 2000; Goldin et al., 2000; Chalmers, 2001; Tang and Lee, 2001; Nguyen and Wereley, 2002; Karniadakis and Beskok, 2002; Madou, 2002; DeGaspari, 2003; Ehrenman, 2004; Sharke, 2004; Stone et al., 2004; Squires and Quake, 2005). Electrostatic, magnetic, electromagnetic, pneumatic and thermal actuators, motors, valves, gears, cantilevers, diaphragms, and tweezers of less than 100 μm size have been fabricated. These have been used as sensors for pressure, temperature, mass flow, velocity, sound, and chemical composition, as actuators for linear and angular motions, and as simple components for complex systems, such as lab-on-a-chip, robots, micro-heat-engines and micro heat pumps (Lipkin, 1993; Garcia and Sniegowski, 1993, 1995; Sniegowski and Garcia, 1996; Epstein and Senturia, 1997; Epstein et al., 1997; Pekola et al., 2004; Squires and Quake, 2005).

Microelectromechanical systems (MEMS) refer to devices that have characteristic length of less than 1 mm but more than 1 micron, that combine electrical and mechanical components, and that are fabricated using integrated circuit batch-processing technologies. The books by Kovacs (1998) and Madou (2002) provide excellent sources for microfabrication technology. Current manufacturing techniques for MEMS include surface silicon micromachining; bulk silicon micromachining; lithography, electrodeposition, and plastic molding (or, in its original German, *Lithographie Galvanoformung Abformung, LIGA*); and electrodischarge machining (EDM). As indicated in Figure 1.1, MEMS are more than four orders of magnitude larger than the diameter of the hydrogen atom, but about four orders of magnitude smaller than the traditional manmade artifacts. Microdevices can have characteristic lengths smaller than the diameter of a human hair. Nanodevices (some say NEMS) further push the envelope of electromechanical miniaturization (Roco, 2001; Lemay et al., 2001; Feder, 2004).

The famed physicist Richard P. Feynman delivered a mere two, albeit profound, lectures[3] on electromechanical miniaturization: "There's Plenty of Room at the Bottom," quoted above, and "Infinitesimal Machinery," presented at the Jet Propulsion Laboratory on February 23, 1983. He could not see a lot of use for micromachines, lamenting in 1959 that "(small but movable machines) may or may not be useful, but they surely would be fun to make," and 24 years later said, "There is no use for these machines, so I still don't

[1] *Gulliver's Travels* were originally designed to form part of a satire on the abuse of human learning. At the heart of the story is a radical critique of human nature in which subtle ironic techniques work to part the reader from any comfortable preconceptions and challenge him to rethink from first principles his notions of man.

[2] The smallest feature on a microchip is defined by its smallest linewidth, which in turn is related to the wavelength of light employed in the basic lithographic process used to create the chip.

[3] Both talks have been reprinted in the *Journal of Microelectromechanical Systems*, vol. 1, no. 1, pp. 60–66, 1992, and vol. 2, no. 1, pp. 4–14, 1993.

understand why I'm fascinated by the question of making small machines with movable and controllable parts." Despite Feynman's demurring regarding the usefulness of small machines, MEMS are finding increased applications in a variety of industrial and medical fields with a potential worldwide market in the billions of dollars.

Accelerometers for automobile airbags, keyless entry systems, dense arrays of micromirrors for high-definition optical displays, scanning electron microscope tips to image single atoms, micro heat exchangers for cooling of electronic circuits, reactors for separating biological cells, blood analyzers, and pressure sensors for catheter tips are but a few of the current usages. Microducts are used in infrared detectors, diode lasers, miniature gas chromatographs, and high-frequency fluidic control systems. Micropumps are used for ink jet printing, environmental testing, and electronic cooling. Potential medical applications for small pumps include controlled delivery and monitoring of minute amount of medication, manufacturing of nanoliters of chemicals, and development of artificial pancreas. The much sought-after lab-on-a-chip is promising to automate biology and chemistry to the same extent the integrated circuit has allowed large-scale automation of computation. Global funding for micro- and nanotechnology research and development quintupled from $432 million in 1997 to $2.2 billion in 2002. In 2004, the U.S. National Nanotechnology Initiative had a budget of close to $1 billion, and the worldwide investment in nanotechnology exceeded $3.5 billion. In 10 to 15 years, it is estimated that micro- and nanotechnology markets will represent $340 billion per year in materials, $300 billion per year in electronics, and $180 billion per year in pharmaceuticals.

The multidisciplinary field has witnessed explosive growth during the past decade. Several new journals are dedicated to the science and technology of MEMS; for example *Journal of Microelectromechanical Systems*, *Journal of Micromechanics and Microengineering*, *Microscale Thermophysical Engineering*, *Microfluidics and Nanofluidics Journal*, *Nanotechnology Journal*, and *Journal of Nanoscience and Nanotechnology*. Numerous professional meetings are devoted to micromachines; for example Solid-State Sensor and Actuator Workshop, International Conference on Solid-State Sensors and Actuators (Transducers), Micro Electro Mechanical Systems Workshop, Micro Total Analysis Systems, and Eurosensors. Several web portals are dedicated to micro- and nanotechnology; for example, <http://www.smalltimes.com>, <http://www.emicronano.com>, <http://www.nanotechweb.org/>, and <http://www.peterindia.net/NanoTechnologyResources.html>.

The three-book *MEMS set* covers several aspects of microelectromechanical systems, or more broadly, the art and science of electromechanical miniaturization. MEMS design, fabrication, and application as well as the physical modeling of their materials, transport phenomena, and operations are all discussed. Chapters on the electrical, structural, fluidic, transport and control aspects of MEMS are included in the books. Other chapters cover existing and potential applications of microdevices in a variety of fields, including instrumentation and distributed control. Up-to-date new chapters in the areas of microscale hydrodynamics, lattice Boltzmann simulations, polymeric-based sensors and actuators, diagnostic tools, microactuators, nonlinear electrokinetic devices, and molecular self-assembly are included in the three books constituting the second edition of *The MEMS Handbook*. The 16 chapters in *MEMS: Introduction and Fundamentals* provide background and physical considerations, the 14 chapters in *MEMS: Design and Fabrication* discuss the design and fabrication of microdevices, and the 15 chapters in *MEMS: Applications* review some of the applications of microsensors and microactuators.

There are a total of 45 chapters written by the world's foremost authorities in this multidisciplinary subject. The 71 contributing authors come from Canada, China (Hong Kong), India, Israel, Italy, Korea, Sweden, Taiwan, and the United States, and are affiliated with academia, government, and industry. Without compromising rigorousness, the present text is designed for maximum readability by a broad audience having engineering or science background. As expected when several authors are involved, and despite the editor's best effort, the chapters of each book vary in length, depth, breadth, and writing style. The nature of the books — being handbooks and not encyclopedias — and the size limitation dictate the noninclusion of several important topics in the MEMS area of research and development.

Our objective is to provide a current overview of the fledgling discipline and its future developments for the benefit of working professionals and researchers. The three books will be useful guides and references

to the explosive literature on MEMS and should provide the definitive word for the fundamentals and applications of microfabrication and microdevices. Glancing at each table of contents, the reader may rightly sense an overemphasis on the physics of microdevices. This is consistent with the strong conviction of the Editor-in-Chief that the MEMS technology is moving too fast relative to our understanding of the unconventional physics involved. This technology can certainly benefit from a solid foundation of the underlying fundamentals. If the physics is better understood, less expensive, and more efficient, microdevices can be designed, built, and operated for a variety of existing and yet-to-be-dreamed applications. Consistent with this philosophy, chapters on control theory, distributed control, and soft computing are included as the backbone of the futuristic idea of using colossal numbers of microsensors and microactuators in reactive control strategies aimed at taming turbulent flows to achieve substantial energy savings and performance improvements of vehicles and other manmade devices.

I shall leave you now for the many wonders of the small world you are about to encounter when navigating through the various chapters of these volumes. May your voyage to Lilliput be as exhilarating, enchanting, and enlightening as Lemuel Gulliver's travels into "Several Remote Nations of the World." *Hekinah degul!* Jonathan Swift may not have been a good biologist and his scaling laws were not as good as those of William Trimmer (see Chapter 2 of *MEMS: Introduction and Fundamentals*), but Swift most certainly was a magnificent storyteller. *Hnuy illa nyha majah Yahoo!*

References

Amato, I. (1998) "Formenting a Revolution, in Miniature," *Science* **282**, no. 5388, 16 October, pp. 402–405.

Angell, J.B., Terry, S.C., and Barth, P.W. (1983) "Silicon Micromechanical Devices," *Faraday Transactions I* **68**, pp. 744–748.

Ashley, S. (1996) "Getting a Microgrip in the Operating Room," *Mech. Eng.* **118**, September, pp. 91–93.

Bryzek, J., Peterson, K., and McCulley, W. (1994) "Micromachines on the March," *IEEE Spectrum* **31**, May, pp. 20–31.

Busch-Vishniac, I.J. (1998) "Trends in Electromechanical Transduction," *Phys. Today* **51**, July, pp. 28–34.

Chalmers, P. (2001) "Relay Races," *Mech. Eng.* **123**, January, pp. 66–68.

DeGaspari, J. (2003) "Mixing It Up," *Mech. Eng.* **125**, August, pp. 34–38.

Ehrenman, G. (2004) "Shrinking the Lab Down to Size," *Mech. Eng.* **126**, May, pp. 26–29.

Epstein, A.H. (2000) "The Inevitability of Small," *Aerospace Am.* **38**, March, pp. 30–37.

Epstein, A.H., and Senturia, S.D. (1997) "Macro Power from Micro Machinery," *Science* **276**, 23 May, p. 1211.

Epstein, A.H., Senturia, S.D., Al-Midani, O., Anathasuresh, G., Ayon, A., Breuer, K., Chen, K.-S., Ehrich, F.F., Esteve, E., Frechette, L., Gauba, G., Ghodssi, R., Groshenry, C., Jacobson, S.A., Kerrebrock, J.L., Lang, J.H., Lin, C.-C., London, A., Lopata, J., Mehra, A., Mur Miranda, J.O., Nagle, S., Orr, D.J., Piekos, E., Schmidt, M.A., Shirley, G., Spearing, S.M., Tan, C.S., Tzeng, Y.-S., and Waitz, I.A. (1997) "Micro-Heat Engines, Gas Turbines, and Rocket Engines — The MIT Microengine Project," AIAA Paper No. 97-1773, AIAA, Reston, Virginia.

Feder, T. (2004) "Scholars Probe Nanotechnology's Promise and Its Potential Problems," *Phys. Today* **57**, June, pp. 30–33.

Feynman, R.P. (1961) "There's Plenty of Room at the Bottom," in *Miniaturization*, H.D. Gilbert, ed., pp. 282–296, Reinhold Publishing, New York.

Gabriel, K.J. (1995) "Engineering Microscopic Machines," *Sci. Am.* **260**, September, pp. 150–153.

Gabriel, K.J., Jarvis, J., and Trimmer, W., eds. (1988) *Small Machines, Large Opportunities: A Report on the Emerging Field of Microdynamics, National Science Foundation*, published by AT&T Bell Laboratories, Murray Hill, New Jersey.

Gabriel, K.J., Tabata, O., Shimaoka, K., Sugiyama, S., and Fujita, H. (1992) "Surface-Normal Electrostatic/Pneumatic Actuator," in *Proc. IEEE Micro Electro Mechanical Systems '92*, pp. 128–131, 4–7 February, Travemünde, Germany.

Garcia, E.J., and Sniegowski, J.J. (1993) "The Design and Modelling of a Comb-Drive-Based Microengine for Mechanism Drive Applications," in *Proc. Seventh International Conference on Solid-State Sensors and Actuators (Transducers '93)*, pp. 763–766, Yokohama, Japan, 7–10 June.

Garcia, E.J., and Sniegowski, J.J. (1995) "Surface Micromachined Microengine," *Sensor. Actuator. A* **48**, pp. 203–214.

Goldin, D.S., Venneri, S.L., and Noor, A.K. (2000) "The Great out of the Small," *Mech. Eng.* **122**, November, pp. 70–79.

Gravesen, P., Branebjerg, J., and Jensen, O.S. (1993) "Microfluidics — A Review," *J. Micromech. Microeng.* **3**, pp. 168–182.

Ho, C.-M., and Tai, Y.-C. (1996) "Review: MEMS and Its Applications for Flow Control," *J. Fluids Eng.* **118**, pp. 437–447.

Ho, C.-M., and Tai, Y.-C. (1998) "Micro–Electro–Mechanical Systems (MEMS) and Fluid Flows," *Annu. Rev. Fluid Mech.* **30**, pp. 579–612.

Hogan, H. (1996) "Invasion of the Micromachines," *New Sci.* **29**, June, pp. 28–33.

Karniadakis, G.E., and Beskok A. (2002) *Microflows: Fundamentals and Simulation*, Springer-Verlag, New York.

Knight, J. (1999) "Dust Mite's Dilemma," *New Sci.* **162**, no. 2180, 29 May, pp. 40–43.

Kovacs, G.T.A. (1998) *Micromachined Transducers Sourcebook*, McGraw-Hill, New York.

Lemay, S.G., Janssen, J.W., van den Hout, M., Mooij, M., Bronikowski, M.J., Willis, P.A., Smalley, R.E., Kouwenhoven, L.P., and Dekker, C. (2001) "Two-Dimensional Imaging of Electronic Wavefunctions in Carbon Nanotubes," *Nature* **412**, 9 August, pp. 617–620.

Lipkin, R. (1993) "Micro Steam Engine Makes Forceful Debut," *Sci. News* **144**, September, p. 197.

Madou, M. (2002) *Fundamentals of Microfabrication*, second edition, CRC Press, Boca Raton, Florida.

Nguyen, N.-T., and Wereley, S.T. (2002) *Fundamentals and Applications of Microfluidics*, Artech House, Norwood, Massachusetts.

O'Connor, L. (1992) "MEMS: Micromechanical Systems," *Mech. Eng.* **114**, February, pp. 40–47.

O'Connor, L., and Hutchinson, H. (2000) "Skyscrapers in a Microworld," *Mech. Eng.* **122**, March, pp. 64–67.

Ouellette, J. (1996) "MEMS: Mega Promise for Micro Devices," *Mech. Eng.* **118**, October, pp. 64–68.

Ouellette, J. (2003) "A New Wave of Microfluidic Devices," *Ind. Phys.* **9**, no. 4, pp. 14–17.

Paula, G. (1996) "MEMS Sensors Branch Out," *Aerospace Am.* **34**, September, pp. 26–32.

Pekola, J., Schoelkopf, R., and Ullom, J. (2004) "Cryogenics on a Chip," *Phys. Today* **57**, May, pp. 41–47.

Robinson, E.Y., Helvajian, H., and Jansen, S.W. (1996a) "Small and Smaller: The World of MNT," *Aerospace Am.* **34**, September, pp. 26–32.

Robinson, E.Y., Helvajian, H., and Jansen, S.W. (1996b) "Big Benefits from Tiny Technologies," *Aerospace Am.* **34**, October, pp. 38–43.

Roco, M.C. (2001) "A Frontier for Engineering," *Mech. Eng.* **123**, January, pp. 52–55.

Sharke, P. (2004) "Water, Paper, Glass," *Mech. Eng.* **126**, May, pp. 30–32.

Sniegowski, J.J., and Garcia, E.J. (1996) "Surface Micromachined Gear Trains Driven by an On-Chip Electrostatic Microengine," *IEEE Electron Device Lett.* **17**, July, p. 366.

Squires, T.M., and Quake, S.R. (2005) "Microfluidics: Fluid Physics at the Nanoliter Scale," *Rev. Mod. Phys.* **77**, pp. 977–1026.

Stone, H.A., Stroock, A.D., and Ajdari, A. (2004) "Engineering Flows in Small Devices: Microfluidics Toward a Lab-on-a-Chip," *Annu. Rev. Fluid Mech.* **36**, pp. 381–411.

Swift, J. (1726) *Gulliver's Travels*, 1840 reprinting of *Lemuel Gulliver's Travels into Several Remote Nations of the World*, Hayward & Moore, London, Great Britain.

Tang, W.C., and Lee, A.P. (2001) "Military Applications of Microsystems," *Ind. Phys.* **7**, February, pp. 26–29.

Tien, N.C. (1997) "Silicon Micromachined Thermal Sensors and Actuators," *Microscale Thermophys. Eng.* **1**, pp. 275–292.

2

Scaling of Micromechanical Devices

William Trimmer
Belle Mead Research, Inc.

Robert H. Stroud
The Aerospace Corporation

2.1 Introduction 2-1
2.2 The Log Plot 2-2
2.3 Scaling of Mechanical Systems 2-3

2.1 Introduction

A revolution in understanding and utilizing micromechanical devices is starting. The utility of these devices will be enormous, and with time they will fill the niches of our lives as pervasively as electronics. What form will these microdevices take? What will actuate them, and how will they interact with their environment? We cannot foresee where the developing technology will take us.

How, then, do we start to design this world of the micro? As you will discover in this book, there are a large number of ways to fabricate microdevices and a vast number of designs. The number of options is greater than we could possibly pursue. Should we just start trying different approaches until something works? Perhaps there is a better way.

Scaling theory is a valuable guide to what may work and what will not. By understanding how phenomena behave and change as their scale size changes, we can gain some insight and better understand the profitable approaches. This chapter examines how things change with size, and it will develop a mathematics that helps find the profitable approaches.

Three general scale sizes will be discussed: astronomical objects; the normal objects we deal with, called macro-objects; and very small objects, called micro-objects. Things that are effective at one of these scale sizes often are insignificant at another scale size. As an example, gravitational forces dominate on an astronomical scale. The motions of our planet around the sun and of our sun around the galaxy are driven mostly by gravitational forces. Yet on the macroscale of my desk top, the gravitational force between two objects such as my tape dispenser and stapler is insignificant. A few simple scaling calculations later in this chapter will tell us this: on astronomical scales, be concerned with gravity; on smaller scales, look to other forces to move objects.

What is obvious on an astronomical-scale size or on a macroscale size is often not obvious on the microscale. For example, take the case of an electric motor. It is really a magnetic motor, and almost all macrosized electric actuators use magnetic fields to generate forces. Hence, one's first intuition would be to use magnetic motors in designing microdevices. In practice, however, most of the common micromotor designs use electrostatic fields instead of magnetic fields. The reasons for this will become obvious in the following discussion of how forces scale.

The field of micromechanical devices is extremely broad. It encompasses all of the traditional science and engineering disciplines, only on a smaller scale. Try to think of a traditional science or engineering discipline that does not have a microequivalent. What we are about in our new discipline is replicating the macroscience and macroengineering on a microscale. As a result, technical people from all science and engineering disciplines can make important contributions to this field.

The time scale from conception to utilization has been collapsing. Alessandro Volta and Andre Marie Ampere developed the basic concepts of electricity, and about 100 years later, Nikola Tesla and Thomas Alva Edison developed practical electric generators and motors. In contrast, the micro-comb-drive motor was described in 1989 and currently is being used in automobiles as an airbag sensor [Tang et al., 1989]. Volta and Ampere's ideas took 100 years to culminate in practical implementation, but the micro-comb-drive motor took less than a dozen years from conception to full-scale implementation.

One of the marvelous things about nature is its widely varying scale sizes. Section 2.2 will discuss this broad range of scales. Section 2.3 will show how scaling theory can be used as a guide to understand how phenomena change with scale. We hope the material that follows encourages you to explore the broad scope of this new field.

2.2 The Log Plot

As the scale, or size, of a system changes by several orders of magnitude, the system tends to behave differently. Consider, for example, a glass of water that is about 5 cm on a side. Pour the glass of water onto a table and notice how the water flows and runs off the edge of the table. If the size of the glass is decreased by two orders of magnitude, or a factor of 100, the glass is now 0.05 cm (or 0.5 mm) on a side. Pour this glass onto the table and see how the surface tension pulls the water into a drop that sticks to the table. Turn the table on its side and observe that it is difficult to make the drop flow to the edge of the table. In each case, the substance is the same, water, and the table is the same, but changing the water's scale size makes it behave very differently.

Decreasing the size of the glass by another two orders of magnitude, the glass is now 0.0005 cm, or 5 μm, on a side. If you try to pour a drop this size onto the table, it most likely will not even reach the table. Some air current will entrain the drop and carry it away like mist flowing through the city at night. Again, the behavior of the water is dramatically different because of its size. Even the act of pouring the glass over the table is different. The 5 cm glass pours, whereas water in the 0.05 cm and 0.0005 cm glasses is constrained by surface tension. Different physical effects manifest themselves differently because of the system size.

Figure 2.1 shows the full range of sizes available to us, from atoms to the universe. Atoms are the smallest mechanical system we will manipulate in the near future; their size is several angstroms (10^{-10} m). The universe is the largest mechanical system we can observe. Depending upon the particular astronomical theory, the universe is about 10^{37} m in diameter. Hence, the full range available for us to investigate and use is about 10^{47} m, or 47 orders of magnitude.

The horizontal axis in Figure 2.1 represents the size of the system. The short vertical lines in the center of the plot represent a factor-of-10 change in the system size. The long vertical lines represent a change of 100,000, or five orders of magnitude. Along the top, the size of the system is given in meters, and in the central band the size of the system is given in angstroms. Figure 2.1 is plotted as a log plot for two reasons: (1) to enable everything to be depicted on the same piece of paper, and (2) to easily portray the different size domains.

One can get a sense of the size of things by looking at the ant, the human, and the whale. These familiar objects span about five orders of magnitude. Several orders of magnitude smaller than the ant are bacteria and viruses. Going to larger systems, the U.S. road system is about five orders of magnitude larger than the whale, and the earth's orbit is about five orders of magnitude larger than the U.S. road system. Increasing another five or six orders of magnitude brings us to interstellar distances.

The bottom portion of Figure 2.1 shows the units we use to measure things. The angstrom, micron, millimeter, meter, kilometer, and mile are familiar units, but then we see a gap of about a dozen orders of magnitude before we reach the astronomical units of the light year and parsec.

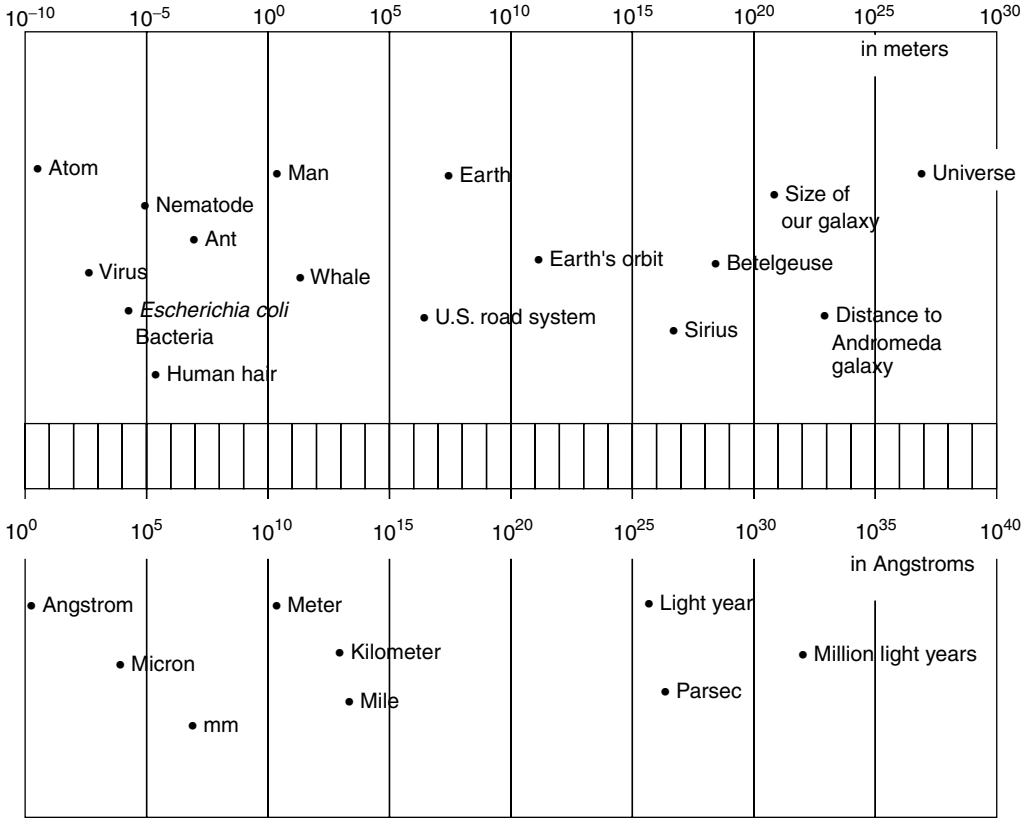

FIGURE 2.1 Log plot of all mechanical systems available for exploration.

The microregion of interest to this chapter ranges from about a millimeter to an angstrom (from about 10^{-3} to 10^{-10} meters). This region comprises roughly a fifth of the full range of domains available for us to explore and may seem like a small portion, but consider that the U.S. roadway system is one of the largest mechanical systems we will build for quite a while. Buildings and ships are probably the largest self-contained mechanical systems we will construct in the near future. Most of the larger domains are so large that they simply are not accessible to us. Thus, the microregion represents the majority of the new domains available for exploration.

This microdomain is enticing. Part of its charm is that conventional designs do not work well, and ingenuity is needed to make new designs. For example, macrodevices and microdevices that transfer water tend to use different physical principles. An open ditch works at one scale, and a capillary works at a smaller scale. Because microdesigners are left without the conventional solutions, they have the opportunity to find their own solutions.

2.3 Scaling of Mechanical Systems

As the size of a system changes, its physical parameters also change, often in a dramatic way [Trimmer et al., 1989; Madou, 1997]. To understand how these parameters change, consider the scale factor *S*. This scale factor is similar to the small notation on the corner of a mechanical drawing that might say the scale of the drawing is 1:10. The actual object to be made is 10 times the size of the drawing. A scale of 1:100 means the actual object is 100 times larger. In the microdomain, the scale might be 100:1, meaning the object is 100 times smaller than the drawing. When the scale size changes, all the dimensions of the object change by exactly the same amount *S* such that 1:*S*.

This scale factor S can be used to describe how physical phenomena change. All the lengths of the drawing scale by the factor S, but other parameters such as the volume scale differently. Volume V is length L times width W times height H, or

$$V = L \cdot W \cdot H \tag{2.1}$$

When the scale changes by 1/100 (that is, decreases by a factor of 100), the length and width and height all change by 1/100, and the volume decreases by $(1/100)^3$ or 1/1,000,000. The volume decreases by a factor of a million when the scale size decreases by a factor of a hundred. Volume is an example of a parameter that scales as S^3. The force due to surface tension scales as S^1; the force due to electrostatics scales as S^2; the force due to certain magnetic forces scales as S^3; and gravitational forces scale as S^4. Now, if the size of the system decreases from a meter to a millimeter, this is a decrease of a factor of a thousand, $S = 1/1000$. The surface tension force decreases by a factor of a thousand, $S^1 = (1/1000)^1$; the electrostatic force decreases by a factor of a million, $S^2 = (1/1000)^2 = 1/1{,}000{,}000$; the magnetic force decreases by a factor of a billion, $S^3 = (1/1000)^3 = 1/1{,}000{,}000{,}000$; and the gravitational force decreases by a factor of a trillion, $S^4 = (1/1000)^4 = 1/1{,}000{,}000{,}000{,}000$. Indeed, changing the size of a mechanical system changes which forces are important.

Knowing how a physical phenomenon scales, whether as S^1 or S^2 or S^3 or S^4 or some other power of S, guides our understanding of how to design small mechanical systems. As an example, consider a water bug. The weight of the water bug scales as the volume, or S^3, while the force used to support the bug scales as the surface tension (S^1) times the distance around the bug's foot (S^1), and the force on the bug's foot scales as $S^1 \times S^1 = S^2$. When the scale size, S, decreases, the weight decreases more rapidly than the surface tension forces. Changing from a 2 m man to a 2 mm bug decreases the weight by a factor of a billion while the surface tension force decreases by a factor of only a million. Hence, the bug can walk on water.

Scaling provides a good guide to how things behave and offers insight into small systems, but scaling is just that — a good guide. It usually does not provide exact solutions. For example, the scaling above does not take into account the difference between the water bug's foot and a person's foot. Water bug's feet are designed for water, and we expect superior performance. Creativity and intuition are what make an excellent design; scaling is a guide to understanding which design elements are important.

A mathematical notation captures the different scaling laws in a convenient form. This notation shows many different scaling laws at once and can be used to easily understand what happens to the different terms and parameters of an equation as the scale size changes.

Consider four different force laws, $F = S^1$, $F = S^2$, $F = S^3$, $F = S^4$, and collect these different cases into a vertical Trimmer bracket:

$$F = \begin{bmatrix} S^1 \\ S^2 \\ S^3 \\ S^4 \end{bmatrix} \tag{2.2}$$

The topmost element of this bracket refers to the case where the force scales as S^1, the next element down refers to the case where the force scales as S^2, and so on.

To continue, let us do something with this bracket. Work W is force F times distance D, or

$$W = F \cdot D \tag{2.3}$$

and, extending our notation,

$$W = F \cdot D = \begin{bmatrix} S^1 \\ S^2 \\ S^3 \\ S^4 \end{bmatrix} \begin{bmatrix} S^1 \\ S^1 \\ S^1 \\ S^1 \end{bmatrix} = \begin{bmatrix} S^2 \\ S^3 \\ S^4 \\ S^5 \end{bmatrix} \tag{2.4}$$

or

$$W = \begin{bmatrix} S^2 \\ S^3 \\ S^4 \\ S^5 \end{bmatrix} \tag{2.5}$$

Note that distance D always scales as S^1, and its bracket consists of all S^1's. In the top case where the force scales as S^1, the distance scales as S^1, and their product scales as S^2. In the second element down, the force scales as S^2, the distance scales as S^1, and their product scales as S^3. Here in one notation we have shown how the work scales for the four different force laws. For example, the gravitational force between an object and the earth scales as S^3 (the earth's mass remains constant in this example, and the mass of the object scales as its volume, S^3). Looking at the third element down, we see that a force scaling of S^3 gives us a work, or energy, scaling of S^4. If the size of a system decreases by a factor of a thousand (say, from 10 cm to 0.10 mm), the gravitational energy required to move an object from the bottom to the top of a machine under consideration decreases by $(1/1000)^4 = 1/1{,}000{,}000{,}000{,}000$. The gravitational work decreases by a factor of a trillion. We know this intuitively: drop an ant from ten times its height, and it walks away. Please do not try this with a horse.

How do the acceleration and transit times change for the different force-scaling laws? Acceleration a is equal to force F divided by the mass m:

$$a = \frac{F}{m} = F \cdot m^{-1} \tag{2.6}$$

and we know the mass scales as S^3, and m^{-1} scales as S^{-3}, giving:

$$a = \begin{bmatrix} S^1 \\ S^2 \\ S^3 \\ S^4 \end{bmatrix} \begin{bmatrix} S^3 \\ S^3 \\ S^3 \\ S^3 \end{bmatrix}^{-1} = \begin{bmatrix} S^1 \\ S^2 \\ S^3 \\ S^4 \end{bmatrix} \begin{bmatrix} S^{-3} \\ S^{-3} \\ S^{-3} \\ S^{-3} \end{bmatrix} = \begin{bmatrix} S^{-2} \\ S^{-1} \\ S^0 \\ S^1 \end{bmatrix} \tag{2.7}$$

This is an interesting result. When the force scales as S^1, the acceleration scales as S^{-2}. If the size of the system decreases by a factor of 100, the acceleration increases by $(1/100)^{-2} = 10{,}000$. As the system becomes smaller, the acceleration increases. A predominance of the forces we use in the microdomain scales as S^2. For these forces, the acceleration scales as S^{-1}, and decreasing the size by a factor of 100 increases the acceleration by a factor of 100, still a nice increase in acceleration. In general, small systems tend to accelerate very rapidly. Where the force scales as S^3, the acceleration remains constant, $(1/100)^0 = 1$, and the acceleration decreases for forces that scale as S^4.

The transit time t to move from point A to B in our scalable drawing can be calculated as:

$$x = \frac{1}{2} at^2 \tag{2.8}$$

$$t = \sqrt{\frac{2x}{a}} = \sqrt{2} \cdot (x)^{0.5} \cdot (a)^{-0.5} \tag{2.9}$$

and

$$t = \begin{bmatrix} S^0 \\ S^0 \\ S^0 \\ S^0 \end{bmatrix} \begin{bmatrix} S^1 \\ S^1 \\ S^1 \\ S^1 \end{bmatrix}^{0.5} \begin{bmatrix} S^{-2} \\ S^{-1} \\ S^0 \\ S^1 \end{bmatrix}^{-0.5} = \begin{bmatrix} S^0 \\ S^0 \\ S^0 \\ S^0 \end{bmatrix} \begin{bmatrix} S^{0.5} \\ S^{0.5} \\ S^{0.5} \\ S^{0.5} \end{bmatrix} \begin{bmatrix} S^1 \\ S^{0.5} \\ S^0 \\ S^{-0.5} \end{bmatrix} = \begin{bmatrix} S^{1.5} \\ S^1 \\ S^{0.5} \\ S^0 \end{bmatrix} \tag{2.10}$$

$$t = \begin{bmatrix} S^{1.5} \\ S^1 \\ S^{0.5} \\ S^0 \end{bmatrix} \tag{2.11}$$

For the case where the force scales as S^2, transit time t scales as S^1. If the system decreases by a factor of 100, the transit time decreases by a factor of 100. Again, we know this intuitively; small things tend to be fast.

Depending upon the equation and variables of interest, the Trimmer brackets can be configured differently. To continue the above example, we might be interested in how things will behave if the acceleration instead of the force scales in different ways. We could write:

$$a = \begin{bmatrix} S^1 \\ S^2 \\ S^3 \\ S^4 \end{bmatrix} \tag{2.12}$$

From above:

$$t = \sqrt{\frac{2x}{a}} = \sqrt{2} \cdot (x)^{0.5} \cdot (a)^{-0.5} \tag{2.13}$$

and

$$t = \begin{bmatrix} S^0 \\ S^0 \\ S^0 \\ S^0 \end{bmatrix} \begin{bmatrix} S^1 \\ S^1 \\ S^1 \\ S^1 \end{bmatrix}^{0.5} \begin{bmatrix} S^1 \\ S^2 \\ S^3 \\ S^4 \end{bmatrix}^{-0.5} = \begin{bmatrix} S^0 \\ S^0 \\ S^0 \\ S^0 \end{bmatrix} \begin{bmatrix} S^{0.5} \\ S^{0.5} \\ S^{0.5} \\ S^{0.5} \end{bmatrix} \begin{bmatrix} S^{-0.5} \\ S^{-1} \\ S^{-1.5} \\ S^{-2} \end{bmatrix} = \begin{bmatrix} S^0 \\ S^{-0.5} \\ S^{-1} \\ S^{-1.5} \end{bmatrix} \tag{2.14}$$

$$t = \begin{bmatrix} S^0 \\ S^{-0.5} \\ S^{-1} \\ S^{-1.5} \end{bmatrix} \tag{2.15}$$

The top element in this bracket describes how time scales when the acceleration scales as S^1. (In the earlier discussion, the top element describes how time scales when the force scales as S^1.) We can arrange these brackets to fit the problem at hand. We need not even use integer exponents. For example, we could have defined the acceleration as:

$$a = \begin{bmatrix} S^{0.1} \\ S^{0.2} \\ S^{0.3} \\ S^2 \\ S^4 \end{bmatrix} \tag{2.16}$$

and then calculated the transit times for these five new scaling functions.

Let us examine the gravitational example in the introduction to this chapter. As we will see in a moment, gravitational forces scale as S^4 and are a dominant force in large systems but not in small systems. The force between two objects is

$$F = G\frac{M_1 \cdot M_2}{r^2} \tag{2.17}$$

where F is the force; G is the gravitational constant ($= 6.670 \times 10^{-11}\,\mathrm{N\,m^2\,kg^{-2}}$), which does not change with scale size; M_1 and M_2 are the masses of the two objects; and r is the separation. The masses scale as:

$$M = \rho \cdot V = S^0 \cdot S^3 = S^3 \tag{2.18}$$

where the density ρ is assumed constant (S^0), and V is the volume (S^3). Now force F scales as:

$$F = S^0\frac{S^3 \cdot S^3}{S^2} = S^4 \tag{2.19}$$

Now, let us make a different assumption and suppose the density is not constant with scale size. The density could be represented as:

$$\rho = \begin{bmatrix} S^0 \\ S^{-1} \\ S^{-2} \\ S^{-3} \end{bmatrix} \tag{2.20}$$

and force F becomes:

$$F = G\frac{M_1 \cdot M_2}{r^2} = G\frac{\rho \cdot V_1 \cdot \rho V_2}{r^2} = G \cdot \rho^2 \cdot V_1 \cdot V_2 \cdot R^{-2} \tag{2.21}$$

$$F = S^0 \begin{bmatrix} S^0 \\ S^{-1} \\ S^{-2} \\ S^{-3} \end{bmatrix} S^3 S^3 S^{-2} = S^0 \begin{bmatrix} S^0 \\ S^{-2} \\ S^{-4} \\ S^{-6} \end{bmatrix} S^3 S^3 S^{-2} = \begin{bmatrix} S^4 \\ S^2 \\ S^0 \\ S^{-2} \end{bmatrix} \tag{2.22}$$

From the top element, where the density does not change with size, the force scales as S^4. From the third element down, when the density scales as S^{-2}, the gravitational force remains constant as the scale size changes. That is, if astronomical objects become less dense as they become larger (as $\rho = S^{-2}$), then the gravitational force between objects remains constant ($F = S^0$) among differently sized astronomical systems.

It is useful to understand how different forces scale. A more complete listing of forces and their scaling is given below,

$$F = \begin{bmatrix} S^1 \\ S^2 \\ S^3 \\ S^4 \end{bmatrix} = \begin{bmatrix} \text{Surface tension} \\ \text{Electrostatic, Pressure, Biological, Magnetic } (J = S^{-1}) \\ \text{Magnetic } (J = S^{-0.5}) \\ \text{Gravitational, Magnetic } (J = S^0) \end{bmatrix} \tag{2.23}$$

Surface tension has the propitious scaling of S^1 and increases rapidly relative to other forces as a system becomes smaller; however, changing the surface tension usually requires changing the temperature, adding a surfactant, or altering some other parameter that is usually difficult to control. Most forces currently used by microdesigners scale as S^2. These include electrostatic forces, forces generated by pressures, and biological forces (the force an animal can exert generally depends upon the cross-section of the muscle). How magnetic forces scale depends upon how the current density (current per unit area of the coils) scales. If the current density J in the coil remains constant (S^0), the magnetic force between two coils scales as S^4, and in this case the magnetic forces become weak in the microdomain; however, we can remove heat much more efficiently from a small volume, and the current density of a microcoil can be much higher than in a large coil. If the current density scales as S^{-1} when the system decreases by a factor of ten, the current density increases by a factor of ten. In this case, the coil has much higher resistive losses, but the force scales much more advantageously as S^2.

References

Madou, M. (1997) *Fundamentals of Microfabrication*, CRC Press, Boca Raton, pp. 405–12.

Tang, W.C., Nguyen, T.-C.H., and Howe, R.T. (1989) "Laterally Driven Polysilicon Resonant Microstructures," *Proceedings of the IEEE Micro Electro Mechanical Systems Workshop*, February 1989; reprinted in *Micromechanics and MEMS: Classic and Seminal Papers to 1990*, W. Trimmer, ed., Institute of Electrical and Electronics Engineers, New York, 1997, pp. 187–93.

Trimmer, W.S.N.T. (1989) "Microrobots and Micromechanical Systems," *Sensor. Actuator.*, September; reprinted in *Micromechanics and MEMS: Classic and Seminal Papers to 1990*, W. Trimmer, ed., Institute of Electrical and Electronics Engineers, New York, 1997, pp. 96–116.

3

Mechanical Properties of MEMS Materials

3.1 Introduction 3-1
3.2 Mechanical Property Definitions 3-2
3.3 Test Methods 3-3
Specimen and Test Structure Preparation • Dimension Measurement • Force and Displacement Measurement • Strain Measurement • Tensile Tests • Bend Tests • Resonant Structure Tests • Membrane Tests • Indentation Tests • Other Test Methods • Fracture Tests • Fatigue Tests • Creep Tests • Round-Robin Tests
3.4 Mechanical Properties 3-16
3.5 Initial Design Values 3-22

William N. Sharpe, Jr.
The Johns Hopkins University

3.1 Introduction

New technologies tend to originate with new materials and manufacturing processes that are used to create new products. In the early stages, the emphasis is on novel devices and systems as well as on ways of making them. Studies of fundamental issues such as mechanical properties and design procedures come later. For example, in 1830 there were 23 miles of railroad track in the U.S., and by 1870 there were 53,000 miles of track. The Bessemer steelmaking process, however, did not originate until 1856, and the American Society for Testing and Materials (ASTM) was not organized until 1898.

The same is true for microelectromechanical systems (MEMS). The emphasis over the past dozen or so years has been on new materials, new manufacturing processes, and new microdevices — and rightfully so. These technological advances have been paralleled by an increasing interest in mechanical testing of materials used in MEMS. More researchers are becoming involved, with the topic appearing in symposia sponsored by the Society for Experimental Mechanics, the American Society of Mechanical Engineers, and the Materials Research Society. Further, the November 2000 ASTM symposium, Mechanical Testing of Structural Films, was an important first step toward standardization of test methods. This increase in MEMS material testing has occurred over the past ten or so years, and this chapter is a review of the current status of the field.

Mechanical properties of interest fall into three general categories: elastic, inelastic, and strength. The designer of a microdevice needs to know its elastic properties in order to predict the amount of deflection from an applied force, or vice versa. If the material is ductile and the deformed structure does not need to return to its initial state, then the designer must know the device's inelastic behavior. The strength of the

material must be known so that the allowable operating limits can be set. The manufacturer of a MEMS device needs to understand the relation between the processing and the properties of the material.

The importance of mechanical properties was recognized early on by a leader in the MEMS field, Richard Muller, who wrote in 1990, "Research on the mechanical properties of the electrical materials forming microdynamic structures (which previously had exclusively electrical uses), on the scaling of mechanical design, and on the effective uses of computer aids is needed to provide the engineering base that will make it possible to exploit fully this technology" [Muller, 1990]. Later, expanded conclusions and recommendations were made in a 1997 report of a National Research Council committee that Muller chaired [Muller, 1997]. One conclusion was, "Test-and-characterization methods and metrologies are required to (1) help fabrication facilities define MEMS materials for potential users, (2) facilitate consistent evaluations of material and process properties at the required scales, and (3) provide a basis for comparisons among materials fabricated at different facilities." One recommendation was, "Studies that address fundamental mechanical properties (e.g., Young's modulus, fatigue strength, residual stress, internal friction) and the engineering physics of long-term reliability, friction, and wear are vitally needed." These rather obvious statements apply to the development of any new technology.

There have been other reviews of the topic. The first on freestanding thin films by Menter and Pashley (1959) is interesting from a historical point of view. This author reviewed existing techniques and introduced new ones in 1996 [Sharpe et al., 1996] and looked at the variation in the mechanical properties of polysilicon as tested by several researchers in 1997 [Sharpe et al., 1997b]. Obermeier (1996) reviewed test methods for mechanical and thermophysical properties. Ballarini (1998) prepared a report for the Air Force Research Laboratory that reviewed pertinent experimental and theoretical work up until then. Yi and Kim (1999a) published a review article, "Measurement of Mechanical Properties for MEMS Materials," on just this topic. Schweitz and Ericson (1999) reviewed the state of the art and offered some interesting conclusions and advice. Chang and Sharpe (1999) wrote an introductory chapter on the subject, and Spearing (2000) wrote a comprehensive exposition from a materials aspect.

This chapter is intended to be a comprehensive survey focusing on both the test methods and the properties that have been measured. After briefly defining the mechanical properties of interest, the chapter reviews the current test methods for MEMS materials. Then, a comprehensive set of tables summarizes the properties of the various materials. In almost all cases, these properties are not yet firmly established with the confidence typical in a handbook, so a final table of initial design values completes the chapter as an aid to initial consideration and design of MEMS.

If the reader is interested in the experimental methods, then the review of test methods will lead to the appropriate references. If the reader desires details about mechanical properties of specific materials, then the tables and the references will prove useful. Finally, if the reader wants to know only the typical properties for an initial design concept, the last section provides a succinct answer.

3.2 Mechanical Property Definitions

The properties of interest here are material properties; that is, the measured value is independent of the test method. Implicit is the understanding that the property is also independent of the size of the specimen, but that may not necessarily be the case for MEMS materials. The fabrication process for, say, thin-film silicon carbide is completely different from that of bulk silicon carbide, and it is reasonable to expect different mechanical behavior. The question of specimen-size effect needs to be considered at the appropriate length scale — in this case, whether a $200 \times 200\,\mu m$ cross-section tensile specimen behaves the same way as a $2 \times 2\,\mu m$ specimen. That question is not very easy to answer until test methods exist with sufficient sensitivity and reproducibility to differentiate the material behavior.

The American Society for Testing and Materials defines standard test procedures through a lengthy process of draft and review. Many of the common standards for structural materials were set in the early part of the twentieth century; however, new standards are established to meet the demands of new technologies, and a complete set of standards is issued each year. For example, the field of fracture mechanics as a usable measure of material and structural response emerged in the early 1950s. The first draft of a standard measure of fracture toughness did not appear until 1965, with the first complete standard appearing in

1970 [ASTM, 1970]. It will be some time before standards for measuring the mechanical properties of MEMS materials are established, but it is useful to be guided by the accepted definitions of mechanical properties. The pertinent standards for testing the mechanical properties of metals appear in [ASTM, 2000a] and those for ceramics in [ASTM, 2000b]. ASTM Standard E-8 gives directions for tension testing of metals, while E-9 covers compression testing. ASTM Standards C-1273 and C-1161 cover the tension and creep testing of ceramics. Once the stress–strain curve is obtained, various approximations, or curve-fits, can be used to insert the material behavior into the design process.

Young's modulus is the slope of the linear part of the stress–strain curve of a material; it is a measure of its stiffness. ASTM E-111 specifies that, "The test specimen is loaded uniaxially and load and strain are measured, either incrementally or continuously." It goes on to prescribe how the slope is determined along with a myriad of other details. Poisson's ratio is a measure of the lateral contraction or expansion of a material when subjected to an axial stress within the elastic region. ASTM E-132 requires that, "In this test method, the value of Poisson's ratio is obtained from strains resulting from uniaxial stress only." Note that these elastic properties are defined for isotropic materials only. Neither of these is easy to measure at the MEMS material size scale, as will be seen in the next section. When a material is inelastic (and nonlinear), we need the complete stress–strain curve to specify the material's behavior.

The strength of a material enables us to determine how much force can be applied to a component or structure. ASTM E-6 defines fracture strength as "the normal stress at the beginning of fracture"; it is the useful measure for brittle materials. ASTM C-1161 defines flexural strength as "a measure of the ultimate strength of a specified beam in bending"; note the linking of the strength measure to a particular size and shape of specimen. If the material is inelastic, then yield strength (defined by a prescribed deviation from initial linearity) defines the departure from elastic response, and tensile strength denotes the maximum stress the material will support before complete failure. Compressive strength is more difficult to establish unless the material is brittle.

Fracture toughness is a generic term for various measures of resistance to extension of a crack. The most familiar measure is plane-strain fracture toughness, ASTM E-399, which requires that the test specimen be thick enough to produce a state of plane strain at the tip of the crack. In this case, the value measured is indeed a material property that is independent of specimen size. Perhaps a more appropriate measure for MEMS is plane-stress fracture toughness, ASTM E-561, but it requires either measuring or inferring the actual crack extension. Implicit in all fracture testing is the condition that the radius at the tip of the crack be very small relative to other dimensions; this is a difficult requirement at the MEMS size scale.

The response of a material to cyclic loading is presented as the S–N curve, which is a plot of the applied stress S on the ordinate vs. the number of cycles to failure N on the abscissa. One obtains such a plot by testing many samples at various levels of applied stress and recording the number of cycles until the specimen breaks in two. ASTM E-466 gives the detailed procedures for metals; this is obviously an expensive test.

Creep is the time-dependent increase in strain under applied stress. Although creep is important in systems operating at high temperature, there is no ASTM standard for creep testing of metals. ASTM C-1291 defines procedures for testing ceramics. As in fatigue testing, results are usually presented in the form of plots.

3.3 Test Methods

Measuring mechanical properties of materials manufactured by processes used in MEMS is not easy. We must be able to: (1) obtain and mount a specimen, (2) measure its dimensions, (3) apply force or displacement to deform it, (4) measure the force, and (5) measure the displacement or, preferably, measure the strain. All of these steps are fully developed and standardized for common structural materials where the minimum dimension of the gauge section of a tensile specimen is 2 mm or so. ASTM E-345 does describe procedures for testing metallic foils that are less than 150 μm thick, but the rest of the dimensions are large. ASTM E-8 includes wires and even describes special grips but does not state a minimum diameter. These two standards offer guidance, but neither is completely appropriate for small MEMS specimens.

The preferred way to determine mechanical properties is by direct methods similar to the approaches of ASTM. To obtain Young's modulus, a uniform stress is applied; it is calculated from direct

measurements of the applied force and the dimensions of the specimen. Strain is measured directly as the force is applied. The specimen is designed to have a uniform gauge section that is long enough to assure that the stress field is not affected by the grip ends and to permit strain measurement. This is not always possible for MEMS materials; in fact, it is most often neither possible nor practical. It is then necessary to resort to inverse methods using a model (simple or complex) of the test structure. Force is applied to the test structure and displacement is measured with the elastic, inelastic, or strength properties then extracted from the model. A simple example that has been widely used in MEMS material testing is a cantilever beam. If it is sufficiently long and thin, then only the Young's modulus enters as a material property into the formula relating force and displacement. Other examples are resonant structures and bulge tests with pressurized membranes; these are described later. If more than one material property appears in the model, then different geometries must be tested.

The formulas for determining Young's modulus, E, by various methods are

Static Beam	Resonant Beam	Bulge Test	Tensile Test
$\frac{4PL^3}{\delta bh^3}$	$\frac{ML^3\omega^2}{2bh^3}$	$\frac{p(1-\nu)a^4}{\delta^3 hc(\nu)}$	$\frac{P}{bh\varepsilon}$

where h, b, and L are the thickness, width, and length of the specimen; P and p are the applied force and pressure; M is the effective mass; ω is the resonant frequency; a is the dimension of a square membrane; and δ and ε are the measured deflection and strain, respectively. The function of Poisson's ratio, $c(\nu)$, depends upon the geometry and is often approximated. The simplicity of the tensile test is an obvious advantage.

Johnson et al. (1999) have compared the uniaxial and bending tests and point out that uncertainty in specimen dimensions is more of a problem in bending tests, while overall elongation is difficult to measure in a tension test. However, if strain can be measured directly, the overall elongation does not need to be measured. Johnson et al. also point out that strength due to misalignment is more of a problem in tension than in bending.

As will be seen later in this chapter, there is an alarming variability among measured values of even so basic a property as Young's modulus for the most widely studied MEMS material — polysilicon. Senturia (1998) attributes this to two primary reasons, "insufficiently precise models used to interpret the data and metrology errors in establishing the geometry of the test devices." He is referring to inverse methods in the first point; whether the boundary conditions of the actual structure actually match the model is a significant question. Senturia's point on metrology applies to all test methods — direct or inverse.

It is useful to distinguish between on-chip test methods and property tests. It is very important in this technology to be able to obtain a measure of mechanical properties from test structures that are on the same chip (or die) as the manufactured MEMS. That usually precludes a direct property measurement on a specimen, which must be larger to allow gripping and pulling even though the size of the gauge section is the same size scale as the microdevice. This is not an issue in mechanical and civil engineering fields, where the required specimen size is smaller than the system or structure. We may regard property tests as basic or baseline and on-chip tests as practical. Obviously, completeness requires direct comparisons of the two approaches with specimens and test structures on the same die.

3.3.1 Specimen and Test Structure Preparation

Microdesign processes cannot take a billet of bulk material and shape it into the final MEMS product as is common for most manufacturing processes. Rather, the microdevice is produced by deposition and etching processes. This means that the specimen or test structure cannot be cut from the bulk material but must be produced by the same processes as the product. A tensile specimen must be designed so that one end remains fixed to the die and the other end accommodates some sort of gripping mechanism. A test structure must be designed so that the boundaries are indeed fixed, and it must incorporate some sort of actuating mechanism to produce force and a sensor to determine displacement or, perhaps, strain.

An early and interesting approach to producing tensile specimens of thin foils was conceived by Neugebauer (1960), who deposited gold films onto oriented rocksalt crystals. The gold film was glued to the grips of a test

machine and the test section covered with sealing wax while the salt was dissolved away. These specimens ranged in thickness from 0.05 to 1.5 μm and were 1–2 mm wide and approximately 1 cm long. Neugebauer found the tensile strength to be two to four times higher than for annealed bulk material but observed no dependence on film thickness. The Young's modulus values agreed with those of the bulk material.

This is a simple example of specimen preparation, but it is illustrative of the methods used in the mechanical test methods for MEMS materials. One deposits the material of interest and removes the unwanted portions of the supporting substrate. An additional step patterns the test material through photolithography.

3.3.2 Dimension Measurement

Minimum features in MEMS are usually on the order of 1 μm — a bit larger than in microelectronics. Measuring the 2×2 μm cross section of a tensile specimen or the equivalent dimensions of a test structure might seem to be easy, but it is not. The thickness of a layer is well controlled and measured by the manufacturer. Lengths are large enough to measure with sufficient accuracy in an optical microscope. It is the width of small specimens or test structure components that is difficult to determine.

A major problem is that the cross-section is not sharply defined or even rectangular as expected. Figure 3.1 is a scanning electron microscope (SEM) photograph of the end of a polysilicon tensile specimen after testing. This specimen is from the Multi-User MEMS Process (MUMPs) process at Cronos, which deposits a first layer of polysilicon that is 2.0 μm thick and then a second layer that is 1.5 μm thick. The interface between these two layers is visible in the photograph. The designed width is 2.0 μm, which is approximately the case at the bottom of the rectangular. The fact that the cross section is not a perfect rectangle contributes to the uncertainty in the area. The corners are somewhat rounded, which makes it difficult to establish the edges when making a plan-view measurement.

The dimensions of a specimen or test structure are normally established before the experiment, but a more accurate measurement may be made after the specimen is broken. Optical or scanning electron microscopy, mechanical or optical profilometry, and interferometry are possible measurement techniques, but some of these can be quite time consuming and expensive. Johnson et al. (1999) state that it is typical to assign an uncertainty of between ± 0.05 and ± 0.10 μm to width measurements. A 2 μm wide

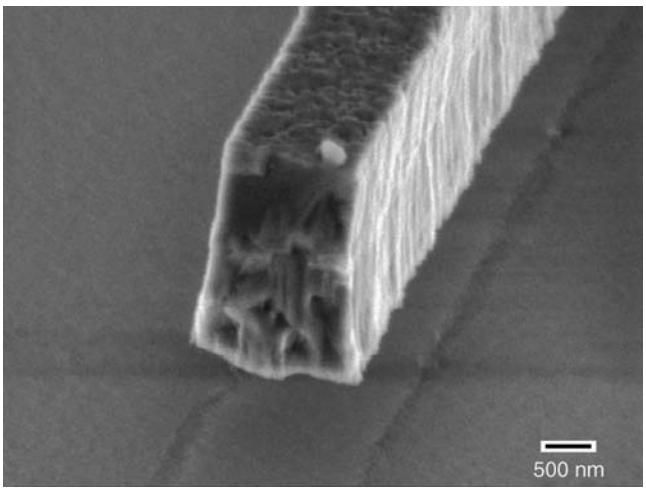

FIGURE 3.1 Scanning electron micrograph of the end of a broken tensile specimen. The specimen is 3.5 mm thick and 2 mm wide at the bottom. (Reprinted with permission from Sharpe et al. [1999a] "Polysilicon Tensile Testing with Electrostatic Gripping," in *Microelectromechanical Structures for Materials Research, Materials Research Society Symposium 518*, pp. 191–96, 15–16 April, San Francisco.).

specimen would therefore have at most ±5% relative uncertainty in its width, which is actually quite reasonable for such small specimens. This reinforces the statement by Senturia (1998) that metrology is a major problem in determining mechanical properties.

3.3.3 Force and Displacement Measurement

Johnson et al. (1999) explain that tensile tests require the measurement of larger forces and smaller overall displacements, while the opposite is true for bending tests. To break a polysilicon tensile specimen $2 \times 2\,\mu m$ square with a fracture strength of 2 GPa requires a force of 8 mN. If that same specimen is 50 μm long, fixed at one end, and with a transverse point load at the other end, breaking it requires a force of only 0.05 mN. If that material has a modulus of 160 GPa, the elongation of a tensile specimen is 0.62 μm, while the deflection at the end of a bending specimen is 10.4 μm.

Commercial force transducers are readily available with a range of ±5 g (50 mN) and a resolution of 0.001 g. This author prefers to use the lower range of a ±100-g load cell because it is stiffer relative to a tensile specimen and to calibrate it with weights. This achieves a resolution of 0.01 g with a full-scale uncertainty of ±1% [Sharpe et al., 1999a]. Howard and Fu (1997) review suitable force transducers, and others, such as Greek et al. (1995) and Saif and MacDonald (1996), construct their own.

Commercial capacitance-based displacement transducers can be used to measure the overall displacement of a test system to a resolution of 0.01 μm and full-scale uncertainty of ±1% [Sharpe et al., 1999a]. Schemes to measure mechanical deflections at the optical microscope level are attractive, and Pan and Hsu (1999) present a vernier gauge approach to measure residual stress. This approach can be electrically instrumented with differential capacitance measurement as shown by Que et al. (1999).

3.3.4 Strain Measurement

It is, of course, preferable to measure strain directly, whether the test arrangement is bending or tension; however, this is difficult to do on such small specimens. The author and his colleagues have developed a laser-based strain-measurement system in which two reflective lines are deposited on the gauge section of a tensile specimen during manufacture. These lines are perpendicular to the loading axis, and when they are illuminated with a low-power laser beam, interference fringe patterns are formed. When the specimen is strained, the lines separate and the fringes move; tracking the motion with diode arrays and a computer system enables real-time strain measurement on specimens as narrow as 20 μm. A set of four lines on wider specimens permits measurement of Poisson's ratio; details are given in Sharpe et al. (1997c; 1997d), and the resolution is approximately ±5 microstrain with a relative uncertainty of 5% at 0.5% strain.

Detailed full-field strain measurements at the MEMS size scale are desirable but difficult. Micro-Raman spectroscopy can probe very small areas on the order of 1 μm in diameter on thin films. Analysis of frequency shifts as force is applied to a specimen leads to local strain measurements [Benrakkad et al., 1995; Pinardi et al., 1997; Zhang et al., 1997; Amimoto et al., 1998]. The moiré method using e-beam lithography to write high-frequency line and dot gratings at a small scale has been demonstrated by Dally and Read (1993), but this is a very challenging process. Chasiotis and Knauss (1998) are developing digital image correlation methods to measure strains in tensile specimens; the resolution is 300–500 microstrain. Mazza et al. (1996a) have demonstrated this to be a viable technique on single-crystal silicon specimens. Laser speckle methods can give full-field results and have been demonstrated by Anwander et al. (2000) and Chang et al. (2000). None of these techniques has been applied to extensive studies of mechanical properties of MEMS materials.

3.3.5 Tensile Tests

Three arrangements are used in tensile tests of MEMS materials: specimen in a supporting frame, specimen fixed to a die at one end; and separate specimen. A fourth clever approach was introduced early on by Koskinen et al. (1993) but has not been continued. They deposited a grid of long, thin tensile specimens that were all fastened to larger portions at each end; the appearance was similar to a foil resistance strain gauge. One end of the arrangement was fixed, and the other was attached to a movable grip that

could be rotated about an axis perpendicular to the grid. This caused all of the specimens to buckle, each a different amount than its neighbor. When the grip moved, each specimen in turn was straightened and pulled. The recorded force-displacement record enabled measurement of modulus and strength.

3.3.5.1 Specimen in Frame

Read and Dally (1992) introduced a very effective way of handling thin-film specimens in 1992. The tensile specimen is patterned onto the surface of a wafer, and then a window is etched in the back of the wafer to expose the gauge section. The result is a specimen suspended across a rectangular frame, which can be handled easily and placed into a test machine. The two larger ends of the frame are fastened to grips, and the two narrower sides are cut to completely free the specimen. This is an extension of the much earlier approach by Neugebauer (1960) and has been adopted by others [Cunningham et al., 1995; Emery et al., 1997; Ogawa et al., 1997; Sharpe et al., 1997c; Cornella et al., 1998; Yi and Kim, 1999b]. A SEM photograph of such a specimen while still in the frame is shown in Figure 3.2.

3.3.5.2 Specimen Fixed at One End

Tsuchiya introduced the concept of a tensile specimen fixed to the die at one end and gripped with an electrostatic probe at the other end [Tsuchiya et al., 1998]. This approach has been adopted by this author and his students [Sharpe et al., 1998a]; Figure 3.3 is a photograph of this type of specimen. The gauge section is 3.5 μm thick, 50 μm wide, and 2 mm long. The fixed end is topped with a gold layer for electrical contact. The grip end is filled with etch holes, as are the two curved transition regions from the grips

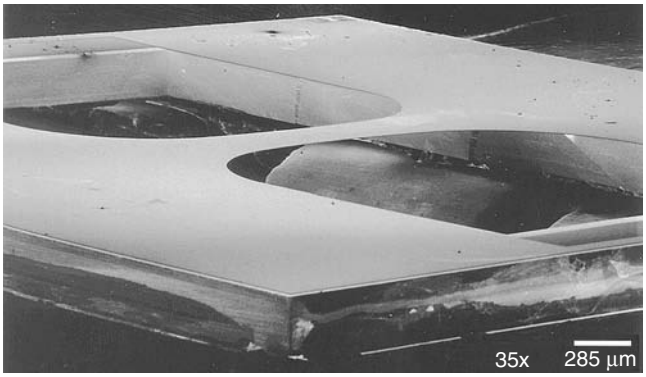

FIGURE 3.2 Scanning electron micrograph of a polysilicon tensile specimen in a supporting single-crystal silicon frame. (Reprinted with permission from Sharpe, W.N., Jr., Yuan, B., Vaidyanathan, R., and Edwards, R.L. [1996] *Proc. SPIE* 2880, pp. 78–91.)

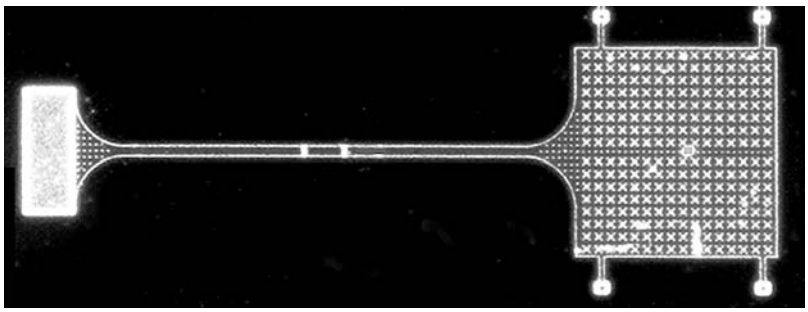

FIGURE 3.3 A tensile specimen fixed at the left end with a free grip end at the right end. (Reprinted with permission from Sharpe, W.N., Jr., and Jackson, K. [2000] *Microscale Systems: Mechanics and Measurements Symposium, Society for Experimental Mechanics,* pp. ix–xiv.)

to the gauge section. The large grip end is held in place during the etch-release process by four anchor straps, which are broken before testing.

Chasiotis and Knauss (2000) have developed procedures for gluing the grip end of a similar specimen to a force/displacement transducer, which enables application of larger forces. A different approach is to fabricate the grip end in the shape of a ring and insert a pin into it to make the connection to the test system. Greek et al. (1995) originated this with a custom-made setup, and LaVan et al. (2000a) use the probe of a nanoindenter for the same purpose.

It is possible to build the deforming mechanism onto or into the wafer, although getting an accurate measure of the forces and deflections can be difficult. Biebl and von Philipsborn (1995) stretched polysilicon specimens in tension with residual stresses in the structure. Yoshioka et al. (1996) etched a hinged paddle in the silicon wafer, which could be deflected to pull a thin single-crystal specimen. Nieva et al. (1998) produced a framed specimen and heated the frame to pull the specimen, as did Kapels et al. (2000).

3.3.5.3 Separate Specimen

The challenge of picking up a tensile specimen only a few microns thick and placing it into a test machine is formidable. However, if the specimens are on the order of tens or hundreds of microns thick, as they are for LIGA-deposited materials, doing so is perfectly possible. This author and his students developed techniques to test steel microspecimens having submillimeter dimensions [Sharpe et al., 1998b]. The steel dog-biscuit-shaped specimens were obtained by cutting thin slices from the bulk material and then cutting out the specimens with a small CNC mill. Electroplated nickel specimens can be patterned into a similar shape in LIGA molds as shown in Figure 3.4. These specimens are released from the substrate by etching, picked up, and put into grips with inserts that match the wedge-shaped ends [Sharpe et al., 1997e].

McAleavey et al. (1998) used the same sort of specimen to test SU-8 polymer specimens. Mazza et al. (1996b) prepared nickel specimens of similar size in the gauge section but with much larger grip ends. Christenson et al. (1998) fabricated LIGA nickel specimens of a more conventional shape; they were approximately 2 cm long with flat grip ends, large enough to test in a commercial table-top electrohydraulic test machine.

3.3.5.4 Smaller Specimens

All of the above methods may appear impressive to the materials test engineer accustomed to common structural materials, but there is a continuing push toward smaller structural components at the nanoscale. Yu et al. (2000) have successfully attached the ends of carbon nanotubes as small as 20 nm in

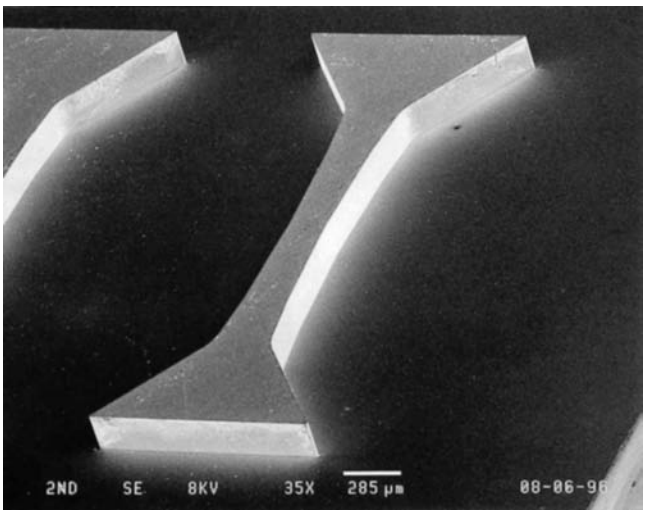

FIGURE 3.4 Nickel microspecimen produced by the LIGA method. The overall length is 3.1 mm, and the width of the specimen at the center is 200 mm. (Reprinted with permission from Sharpe, W.N., Jr., et al. [1997] *Proc. Int. Solid State Sensors and Actuators Conf. — Transducers '97*, pp. 607–10. © 1997 IEEE.)

diameter and a few microns long to atomic force microscopy (AFM) probes. As the probes are moved apart inside a SEM, their deflections are measured and used to extract both the force in the tube and its overall elongation. They report strengths up to 63 GPa and modulus values up to 950 GPa.

3.3.6 Bend Tests

Three arrangements are also used in bend tests of structural films: out-of-plane bending of cantilever beams, beams fastened at both ends, and in-plane bending of beams. Larger specimens, which can be individually handled, can also be tested in bending fixtures similar to those used for ceramics.

3.3.6.1 Out-of-Plane Bending

The approach here is simple. The process patterns long, narrow, and thin beams of the test material onto a substrate and then etches away the material underneath to leave a cantilever beam hanging over the edge. By measuring the force vs. deflection at or near the end of the beam, one can extract Young's modulus via the formula in section 3.3. However, this is difficult because if the beams are long and thin, the deflections can be large, but the forces are small. The converse is true if the beam is short and thick, but then the applicability of simple beam theory comes into question. If the beam is narrow enough, Poisson's ratio does not enter the formula; otherwise, beams of different geometries must be tested to determine it.

Weihs et al. (1988) introduced this method in 1988 by measuring the force and deflection with a nanoindenter having a force resolution of 0.25 μN and a displacement resolution of 0.3 nm. Typical specimens had a thickness, width, and length of 1.0, 20, and 30 μm, respectively. Figure 3.5 shows a cantilever beam deflected by a nanoindenter tip in a later investigation [Hollman et al., 1995].

Biebl et al. (1995a) attracted the end of a cantilever down to the substrate with electrostatic forces and recorded the capacitance change as the voltage was increased to pull more of the beam into contact. Fitting these measurements to an analytical model permitted a determination of Young's modulus.

Krulevitch (1996) proposed a technique for measuring Poisson's ratio of thin films fabricated in the shapes of beams and plates by comparing the measured curvatures. These were two-layer composite

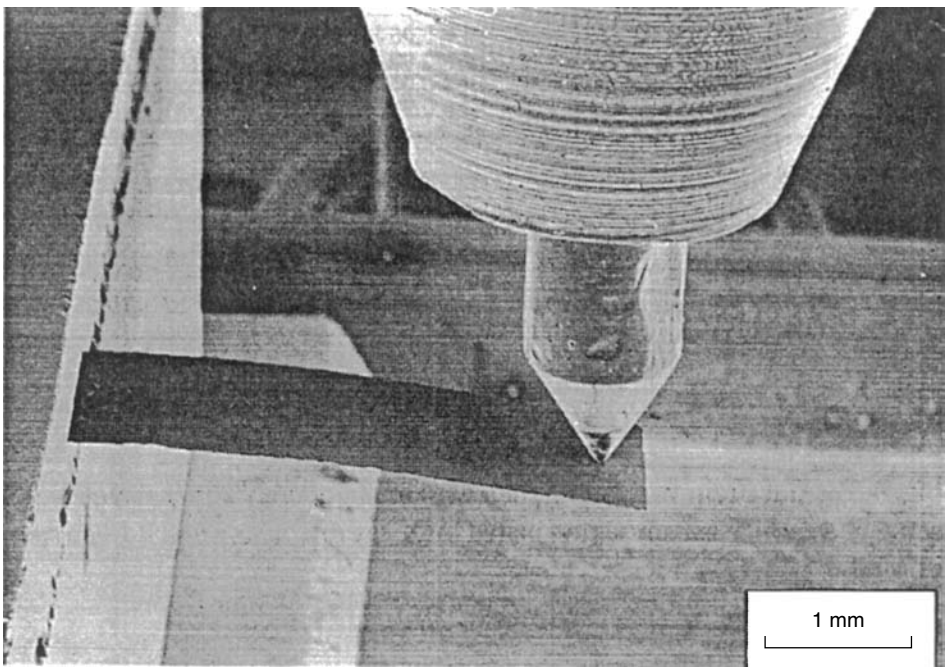

FIGURE 3.5 A cantilever microbeam deflected out of plane by a diamond stylus. The beam was cut from a free-standing diamond film. (Reprinted with permission from Hollman, P., et al. (1995) "Residual Stress, Young's Modulus and Fracture Stress of Hot Flame Deposited Diamond," *Thin Solid Films* **270**, pp. 137–42.)

structures, so the properties of the substrate must be known. Kraft et al. (1998) also tested composite beams by measuring the force-deflection response with a nanoindenter. Bilayer cantilever beams have been tested by Tada et al. (1998), who heated the substrate and measured the curvature.

More sensitive measurements of force and displacement on smaller cantilever beams can be made by using an AFM probe, as shown by Serre et al. (1998), Namazu et al. (2000), Comella and Scanlon (2000), and Kazinczi et al. (2000). A specially designed test machine using an electromagnetic actuator has been developed by Komai et al. (1998).

3.3.6.2 Beams with Fixed Ends

Working with a beam that is fixed at both ends is somewhat easier; the beam is stiffer and more robust. Tai and Muller (1990) used a surface profilometer to trace the shapes of fixed-fixed beams at various load settings. By comparing measured traces and using a finite element analysis of the structure, they were able to determine Young's modulus.

A promising on-chip test structure has been developed over the years by Senturia and his students; it is shown schematically in Figure 3.6. A voltage is applied between the conductive polysilicon beam and the substrate to pull the beam down, and the voltage that causes the beam to make contact is a measure of its stiffness. This concept was introduced early on by Petersen and Guarnieri (1979) and further developed by Gupta et al. (1996). A similar approach and analysis were described by Zou et al. (1995). The considerable advantage here is that the measurements can be made entirely with electrical probing in a manner similar to that used to check microelectronic circuits. This opens the opportunity for process monitoring and quality control.

The fixed ends clearly exert a major influence on the stiffness of the test structure. Kobrinsky et al. (1999) have thoroughly examined this effect and shown its importance. The problem is that a particular manufacturing process, or even variations within the same process, may etch the substrate slightly differently and change the rigidity of the ends. Nevertheless, this is a potentially very useful method for monitoring the consistency of MEMS materials and processes.

Zhang et al. (2000) recently conducted a thorough study of silicon nitride in which microbridges (fixed–fixed beams) were deflected using a nanoindenter with a wedge-shaped indenter. By fitting the measured force-deflection records to their analytical model, they extracted both Young's modulus and residual stress.

3.3.6.3 In-Plane Bending

In-plane bending may be a more appropriate test method in that the structural supports of MEMS accelerometers are subjected to that mode of deformation. Jaecklin et al. (1994) pushed long, thin cantilever beams with a probe until they broke; optical micrographs gave the maximum deflections, from which the fracture

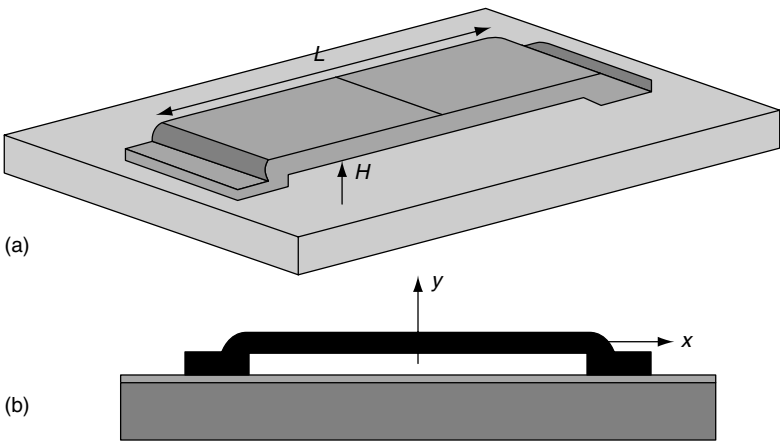

FIGURE 3.6 Schematic of a fixed-fixed beam. (Reprinted with permission from Kobrinsky, M. et al. [1999] "Influence of Support Compliance and Residual Stress on the Shape of Doubly-Supported Surface Micromachined Beams," *MEMS Microelectromechanical Systems* **1**, pp. 3–10, ASME, New York.)

strain was determined. Jones et al. (1996) constructed a test structure consisting of cantilever beams of different lengths fastened to a movable shuttle. As the shuttle was pushed, the beams contacted fixed stops on the substrate; the deformed shape was videotaped and the fracture strain determined. Figure 3.7 is a photograph of one of their deformed specimens.

Kahn et al. (1996) developed a double cantilever beam arrangement to measure the fracture toughness of polysilicon and used the measured displacement between the two beams to determine Young's modulus via a finite element model. The beams were separated by forcing a mechanical probe between them and pushing it toward the notched end. Fitzgerald et al. (1998) have taken a similar approach to measure crack growth and fracture toughness in single-crystal silicon, but they use a clever structure that permits opening the beams by compression of cantilever extensions.

3.3.6.4 Bending of Larger Specimens

Microelectromechanical technology is not restricted to thin-film structures, although they are far-and-away predominant. Materials fabricated with thicknesses on the order of tens or hundreds of microns are of current interest and likely to become more important in the future.

Ruther et al. (1995) manufactured a microtesting system using the LIGA process to test electroplated copper. The interesting feature is that the in-plane cantilever beam and the test system are fabricated together on the die; however, this requires a rather complex assembly. Stephens et al. (1998) fabricated rows of LIGA nickel beams sticking up from the substrate and then measured the force applied near the upper tip of the beam while displacing the substrate. The resulting force-displacement curve permitted extraction of Young's modulus, and the recorded maximum force gave a modulus of rupture.

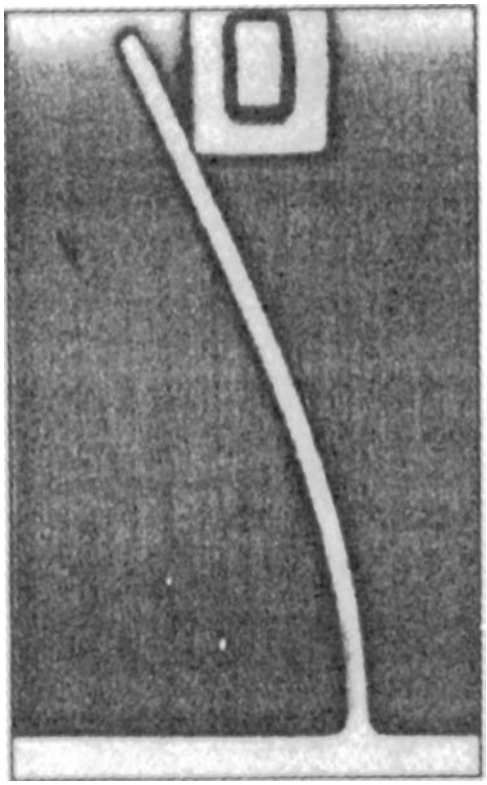

FIGURE 3.7 A polysilicon cantilever beam subjected to in-plane bending. The beam is 2.8 mm wide, and the vertical distance between the fixed end at the bottom and the deflected end at the top is 70 mm. (Reprinted with permission from Sharpe, W.N., Jr., et al. [1998] "Round-Robin Tests of Modulus and Strength of Polysilicon," *Microelectromechanical Structures for Materials Research Symposium*, pp. 56–65.)

Larger structures, such as the microengine under development at the Massachusetts Institute of Technology, have thicknesses on the order of several millimeters. It then becomes necessary to test specimens of similar sizes in what is sometimes called the mesocale region, whose dimensions generally range from 0.1 mm to 1 cm. Single-crystal silicon is the material of interest for initial versions, and Chen et al. (1998) have developed a method for bend testing square plates simply supported over a circular hole and recording the force as a small steel ball is pushed into the center of the plate. Fracture strengths are obtained, and this efficient arrangement permits study of the effects of various manufacturing processes on the load-carrying capability of the material.

3.3.7 Resonant Structure Tests

Frequency and changes in frequency can be measured precisely, and elastic properties of modeled structures can be determined. The microstructures can be very small and excited by capacitive comb-drives, which require only electrical contact. This makes this approach suitable for on-chip testing; in fact, the MUMPs process at Cronos includes a resonant structure on each die. That microstructure moves parallel to the substrate, but others vibrate perpendicularly.

Petersen and Guarnieri (1979) introduced the resonant structure concept in 1979 by fabricating arrays of thin, narrow cantilever beams of various lengths extending over an anisotropically etched pit in the substrate. The die containing the beams was excited by variable frequency electrostatic attraction between the substrate and the beams, and the vibration perpendicular to the substrate was measured by reflection from an incident laser beam, as shown by the schematic in Figure 3.8. Yang and Fujita (1997) used a similar approach to study the effect of resistive heating on U-shaped beams. Commercial AFM cantilevers were tested in a similar manner by Hoummady et al. (1997), who measured the higher resonant modes of a cantilever beam with a mass on the end. Zhang et al. (1991) measured vibrations of a beam fixed at both ends by using laser interferometry. Michalicek et al. (1995) developed an elaborate and carefully modeled micromirror that was excited by electrostatic attraction. Deflection was also measured by laser interferometry, and experiments determined Young's modulus over a range of temperatures as well as validating the model.

Microstructures that vibrate parallel to the plane of the substrate require less processing because the substrate does not have to be removed. Biebl et al. (1995b) introduced this concept, and Kahn et al. (1998) have used a more recent version to study the effects of heating on the Young's modulus of films sputtered

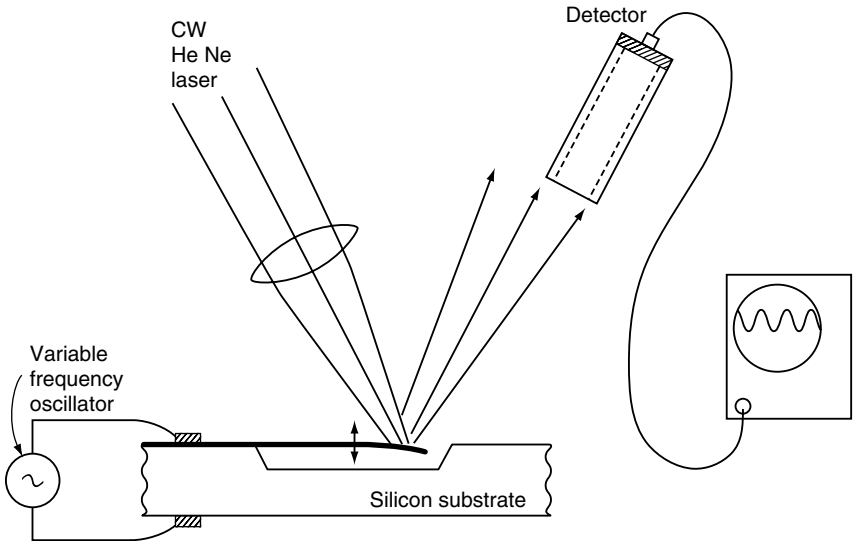

FIGURE 3.8 Schematic of the resonant structure system of Petersen and Guarnieri (1979). (Reprinted with permission from Petersen, K.E., and Guarnieri, C.R. [1979] "Young's Modulus Measurements of Thin Films Using Micromechanics," *J. Appl. Phys.* **50**, pp. 6761–66.)

onto the structure. Figure 3.9 is a SEM image of their structure, which is easy to model. Pads A, B, C, and D are fixed to the substrate; the rest of the structure is free. Electrostatic comb-drives excite the two symmetrical substructures, which consist of four flexural springs and a rigid mass. The resonant frequency of this device is around 47 kHz. Brown et al. (1997) have developed a different approach in which a small notched specimen is fabricated as part of a large resonant fan-shaped component. This resonant structure, shown in Figure 3.10, has been used primarily for fatigue and crack growth studies,

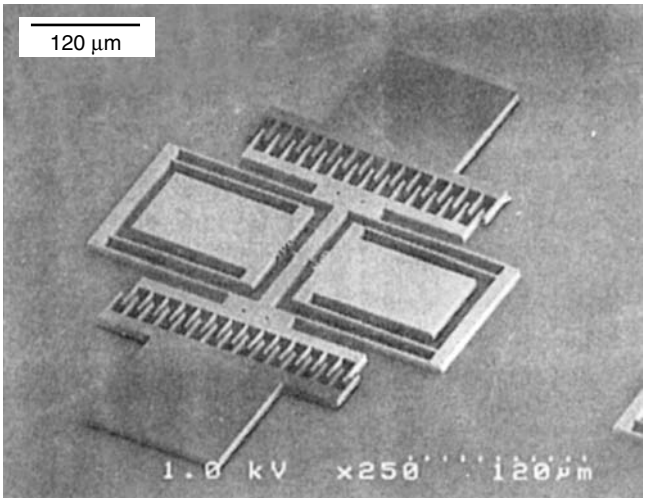

FIGURE 3.9 Scanning electron micrograph of the in-plane resonant structure of Kahn et al. (1998). (Reprinted with permission from Kahn, H. et al. [1998] "Heating Effects on the Young's Modulus of Films Sputtered onto Micromachined Resonators," *Microelectromechanical Structures for Materials Research Symposium,* pp. 33–38.)

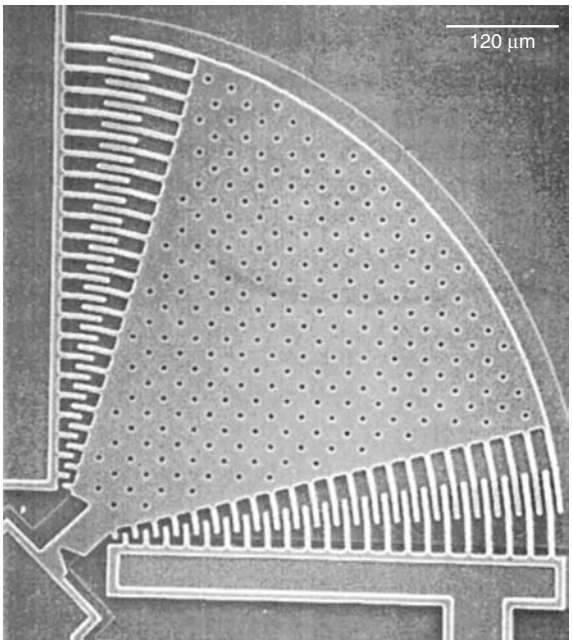

FIGURE 3.10 Scanning electron micrograph of the in-plane resonant structure of Brown et al. (1997). (Reprinted with permission from Brown, S.B. et al. [1997] "Materials Reliability in MEMS Devices," *Proc. Int. Solid-State Sensors and Actuators Conf. — Transducers '97*, pp. 591–93. © 1997 IEEE.)

but Young's modulus of polysilicon has been extracted from its finite element model [Sharpe et al., 1998c].

3.3.8 Membrane Tests

It is relatively easy to fabricate a thin membrane of test material by etching away the substrate; the membrane is then pressurized and the measured deflection can be used to determine the biaxial modulus. An advantage of this approach is that tensile residual stress in the membrane can be measured, but the value of Poisson's ratio must be assumed. This method, often called bulge testing, was first introduced by Beams (1959), who tested thin films of gold and silver and measured the center deflection of the circular membrane as a function of applied pressure. Jacodine and Schlegel (1966) used this approach to measure Young's modulus of silicon oxide. Tabata et al. (1989) tested rectangular membranes whose deflections were measured by observations of Newton's rings, as did Maier-Schneider et al. (1995). The variation of Hong et al. (1990) used circular membranes with force deflection measured at the center with a nanoindenter. Pressurized square membranes with the deflection measured by a stage-mounted microscope were tested by Walker et al. (1990) to study the effect of hydrofluoric acid exposure on polysilicon; a similar approach to determine biaxial modulus, residual stress, and strength was used by Cardinale and Tustison (1992). Vlassak and Nix (1992) eliminated the need to assume a value of Poisson's ratio by testing rectangular silicon nitride films with different aspect ratios. More recently, Jayaraman et al. (1998) used this same approach to measure Young's modulus and Poisson's ratio of polysilicon.

3.3.9 Indentation Tests

A nanoindenter is, in the fewest words, simply a miniature and highly sensitive hardness tester. It measures both force and displacement, and modulus and strength can be obtained from the resulting plot. Penetration depths can be very small (a few nanometers), and automated machines permit multiple measurements to enhance confidence in the results and also to scan small areas for variations in properties.

Weihs et al. (1989) measured the Young's modulus of an amorphous silicon oxide film and a nontextured gold film with a nanoindenter and obtained only limited agreement with their microbeam deflection experiments. The modulus measured by indentation was consistently higher, and the large pressure of the indenter tip was the probable cause. Taylor (1991) used nanoindenter measurements restricted to penetrations of 200 nm into silicon nitride films 1 μm thick to study the effects of processing on mechanical properties. Young's modulus decreased with decreasing density of the films.

Bhushan and Li (1997) have studied the tribological properties of MEMS materials, and Li and Bhusan (1999) used a nanoindenter to measure the modulus and a microhardness tester to measure the fracture toughness of thin films. Measurements of Young's modulus of polysilicon showed a wide scatter. Bucheit et al. (1999) examined the mechanical properties of LIGA-fabricated nickel and copper by using a nanoindenter as one of the tools. In most cases, Young's modulus from nanoindenter measurements were higher than from tension tests, but the nanoindenter does allow looking at both sides of the thin film as well as at sectioned areas.

3.3.10 Other Test Methods

The readily observed buckling of a column-like structure under compression can be used to measure forces in specimens; if the specimen breaks, the fracture strength can be estimated. Tai and Muller (1988) fabricated long, thin polysilicon specimens with one end fixed and the other enclosed in slides. The movable end was pushed with a micromanipulator, and its displacement when the structure buckled was used to determine the strain (not stress) at fracture. Ziebart and colleagues have analyzed thin films with various boundary conditions ranging from fixed along two sides [Ziebart et al., 1997] to fixed on all four sides [Ziebart et al., 1999]. The first arrangement permitted the measurement of Poisson's ratio when the side supports were compressed, and the second determined prestrains induced by processing. Beautiful patterns are obtained, but the analysis and the specimen preparation can be time consuming.

Another clever approach based on buckling is described by Cho et al. (1997). They etched away the silicon substrate under an overhanging strip of diamond-like carbon film and used the buckled pattern to determine the residual stress in the film. A more traditional creep test was used by Teh et al. (1999) to study creep in $2 \times 2 \times 100\,\mu m$ polysilicon strips fixed at each end. As current passed through the specimens, they heated up, and their buckled deflection over time at a constant current was used to extract a strain-vs.-time creep curve. This approach is complicated by the nonuniformity of the strain in the specimen.

Although torsion is an important mode of deformation in certain MEMS, such as digital mirrors, few test methods have been developed. Saif and MacDonald (1996) introduced a system to twist very small ($10\,\mu m$ long and $1\,\mu m$ on a side) pillars of single-crystal silicon and measure both the force and deflection. Larger ($300\,\mu m$ long with side dimensions varying from 30 to $180\,\mu m$) of both silicon and LIGA nickel were tested by Schiltges et al. (1998). Emphasis was on the elastic properties only with the shear modulus values agreeing with expected bulk values.

Nondestructive measurements of elastic properties of thin films can be accomplished with laser-induced ultrasonic surface waves. A laser pulse generates an impulse in the film, and a piezoelectric transducer senses the surface wave. In principle, Young's modulus, density, and thickness can be determined, but this cannot be achieved for all combinations of film and substrate materials. Schneider and Tucker (1996) describe this test method and present results for a wide range of films; the Young's modulus values generally agree with other thin-film measurements. A drawback here is the planar size of the film; the input and output must be several millimeters apart. A related technique uses Brillouin scattering as described in Monteiro et al. (1996).

3.3.11 Fracture Tests

Single-crystal silicon and polysilicon are both brittle materials, and it is therefore natural to want to measure their fracture toughness. This is even more difficult than measuring their fracture strength because of the need for a crack with a tip radius that is small relative to the specimen dimensions.

Photolithography processes for typical thin films have a minimum feature radius of approximately 1 mm. Fan et al. (1990), Sharpe et al. (1997f) and Tsuchiya et al. (1998) have tested polysilicon films in tension using edge cracks, center cracks, and edge cracks, respectively. Kahn et al. (1999) modeled a double-cantilever specimen with a long crack and wedged it open with an electrostatic actuator.

Fitzgerald et al. (1999) prepared sharp cracks in double-cantilever silicon crystal specimens by etching, and Suwito et al. (1997) modeled the sharp corner of a tensile specimen to measure the fracture toughness. Van Arsdell and Brown (1999) introduced cracks at notches in polysilicon with a diamond indenter. A promising new approach using a focused ion beam (FIB) can prepare cracks with tip radii of 30 nm according to K. Jackson (pers. comm.).

3.3.12 Fatigue Tests

Many MEMS operate for billions of cycles, but that kind of testing is conducted on microdevices, such as digital mirrors instead of the more basic reversed bending or push–pull tests so familiar to the metal fatigue community. Brown and his colleagues have developed a fan-shaped, electrostatically driven notched specimen that has been used for fatigue and crack growth studies [Brown et al., 1993, 1997; Van Arsdell and Brown, 1999]. Minoshima et al. (1999) have tested single-crystal silicon in bending fatigue, and Sharpe et al. (1999) reported some preliminary tension–tension tests on polysilicon. As noted earlier, fatigue data are reported as stress-vs.-life plots, and Kapels et al. (2000) present a plot that looks much like one would expect for a metal; the allowable applied stress decreases from 2.9 GPa for a monotonic test to 2.2 GPa at one million cycles.

3.3.13 Creep Tests

Some MEMS are thermally actuated, so the possibility of creep failure exists. No techniques similar to the familiar dead-weight loading to produce strain-vs.-time curves exist. Teh et al. (1999) have observed the buckling of heated fixed-end polysilicon strips.

3.3.14 Round-Robin Tests

Mechanical testing of MEMS materials presents unique challenges as the above review shows. Convergence of test methods into a standard is still far in the future, but progress in that direction usually begins with a round-robin program in which a common material is tested by the method-of-choice in participating laboratories. That first step was taken in 1997/1998 with the results reported at the Spring 1998 meeting of the Materials Research Society [Sharpe et al., 1998c]. Polysilicon from the MUMPs 19 and 21 runs of Cronos were tested in bending (Figure 3.7), resonance (Figure 3.10), and tension (Figure 3.3). Young's modulus was measured as 174 ± 20 GPa in bending, 137 ± 5 GPa in resonance, and 139 ± 20 GPa in tension. Strengths in bending were 2.8 ± 0.5 GPa, in resonance 2.7 ± 0.2 GPa, and in tension 1.3 ± 0.2 GPa. These variations were alarming but in retrospect perhaps not too surprising given the newness of the test methods at that time.

A more recent interlaboratory study of the fracture strength of polysilicon manufactured at Sandia has been arranged by LaVan et al. (2000b). Strengths measured on similar tensile specimens by Tsuchiya in Japan and at Johns Hopkins were 3.23 ± 0.25 and 2.85 ± 0.40 GPa respectively. LaVan tested in tension with a different approach and obtained 4.27 ± 0.61 GPa. It seems clear that more effort needs to be devoted to the development of test methods that can be used in a standardized manner by anyone who is interested.

3.4 Mechanical Properties

This section lists in tabular form the results of measurements of mechanical properties of materials used in MEMS structural components. Its intent is not only to provide values of mechanical properties but also to supply references on materials and test methods of interest. Because as yet no standard test method exists and such a wide variety in the values is obtained for supposedly identical materials, readers with a strong interest in the mechanical behavior of a particular material can use the tables to identify pertinent references.

Almost all the data listed comes from experiments directly related to free-standing structural films. The only exceptions are the results from ultrasonic measurements by Schneider and Tucker (1996) because they tested a number of materials of interest. Including information on the processing conditions for each reference proved too cumbersome, but the short comments in the tables should be useful. Many of the results are average values of multiple replications, and the standard deviations are included when they are available. Most of the materials used in MEMS are ceramics and show linear and brittle behavior, in which case only the fracture strength is listed. The tables for ductile materials show both yield and ultimate strengths. Also note that the values in the tables are edited from a larger list. Some of the same values have been presented in two different venues (e.g., a conference publication and a journal paper), in which case the more archival version was referenced. A limited number of studies have been conducted on the effects of environment (temperature, hydrofluoric acid, saltwater, etc.) on MEMS materials, but that area of research is in its infancy and is not included.

First, typical stress–strain curves are plotted in Figure 3.11 to compare the mechanical behavior of MEMS materials with a common structural steel, A533-B, which is moderately strong (yield strength of 440 MPa) but ductile and tough. Polysilicon is linear and brittle and much stronger. LIGA nickel is ductile and considerably stronger than bulk pure nickel. One must test materials as they are produced for MEMS instead of relying on bulk material values.

The microstructure of these MEMS materials is also different from that of bulk materials. The physics of the thin-film deposition process cause the grains to be columnar in a direction perpendicular to the film as shown in Figure 3.12. The result is similar to the cross-section of a piece of bamboo or wood, and the material is transversely isotropic. Test methods are not sensitive enough to measure the anisotropic constants.

Table 3.1 lists metal films tested in a free-standing manner such as would be appropriate for use in MEMS. Only aluminum is currently used in that fashion, but the other materials are commonly used in the electronics industry and may be of interest. Note that all of the materials are ductile; the complete stress–strain curves are included in many of the references. The values of Young's modulus as measured for pure bulk materials are listed for reference.

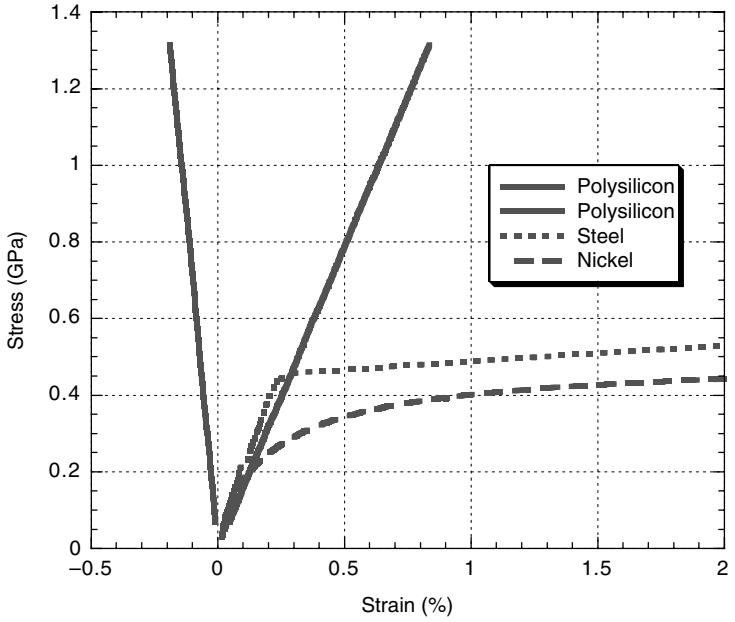

FIGURE 3.11 Representative stress–strain curves of polysilicon, electroplated nickel, and A-533B steel. These are from microspecimens tested in the author's laboratory.

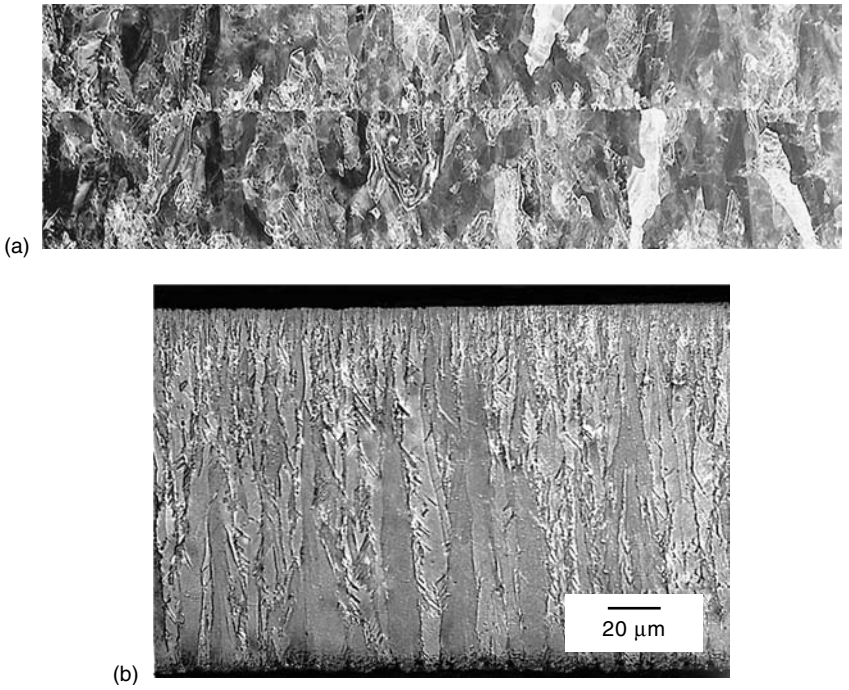

FIGURE 3.12 Microstructure of two common MEMS materials. Note the columnar grain structure perpendicular to the plane of the film. (a) Polysilicon deposited in two layers; the bottom layer is 2.0 μm thick and the top one is 1.5 μm thick. (Reprinted with permission from Sharpe et al. [1998c] "Round-Robin Tests of Modulus and Strength of Polysilicon," in *Microelectromechanical Structures for Materials Research, Materials Research Society Symposium 518*, pp. 56–65, 15–16 April, Francisco. © 1998 IEEE.) (b) Nickel electroplated into LIGA molds. (Reprinted with permission from Sharpe et al. [1997d] "Measurements of Young's Modulus, Poisson's Ratio, and Tensile Strength of Polysilicon," *Proc. IEEE Tenth Annual Int. Workshop on Micro Electro Mechanical Systems*, pp. 424–29, 26–30 January, Nagoya, Japan. © 1998 IEEE.)

TABLE 3.1 Metals

Metals	Young's Modulus (GPa)	Yield Strength (GPa)	Ultimate Strength (GPa)	Method	Comments	Ref.
Aluminum	8–38	—	0.04–0.31	Tension	110–160 μm thick	Hoffman (1989)
modulus of bulk material = 69 GPa	40	—	0.15	Tension	1.0 μm thick	Ogawa et al. (1996)
	69–85	—	—	Bending	Various lengths	Comella and Scanlon (2000)
Copper	86–137	0.12–0.24	0.33–0.38	Tension	Plated; annealed	Buchheit et al. (1999)
modulus of bulk material = 117 GPa	108–145	—	—	Indentation	Various locations	Buchheit et al. (1999)
	98 ± 4	—	—	Tension	Laser speckle	Anwander et al. (2000)
Gold	40–80	—	0.2–0.4	Tension	0.06–16 μm thick	Neugebauer (1960)
modulus of bulk material = 74 GPa	57	0.26	—	Bending	~1 μm thick	Weihs et al. (1988)
	74	—	—	Indentation	~1 μm thick	Weihs et al. (1988)
	82	—	0.33–0.36	Tension	0.8 μm thick	Emery et al. (1997)
	—	—	0.22–0.27	Bending	Composite beam	Kraft et al. (1998)
Titanium						
modulus of bulk material = 110 GPa	96 ± 12	—	0.95 ± 0.15	Tension	0.5 μm thick	Ogawa et al. (1997)
Ti–Al–Ti	—	0.07–0.12	0.14–0.19	Tension	Composite film	Read and Dally (1992)

TABLE 3.2 Diamond-Like Carbon

Young's Modulus (GPa)	Fracture Strength (GPa)	Method	Comments	Ref.
600–1100	0.8–1.8	Bending	Hot flame deposited	Hollman et al. (1995)
800–1140	—	Ultrasonic	CVD diamond	Schneider and Tucker (1996)
150–800	—	Ultrasonic	Laser arc deposited	Schneider and Tucker (1996)
580	—	Brillouin	CVD diamond	Monteiro et al. (1996)
94–128	—	Buckling	Poisson's ratio = 0.22	Cho et al. (1998)
—	8.5 ± 1.4	Tension	Amorphous diamond	LaVan et al. (2000a)

Carbon can be deposited to form an amorphous or crystalline structure that is often referred to as diamond-like carbon, (DLC). Diamond itself has a very high stiffness and strength as well as a low coefficient of friction; for these reasons DLC offers exciting possibilities in MEMS. The very limited results to date, shown in Table 3.2, support this line of reasoning although they are far too sparse to be conclusive.

Electroplated nickel and nickel–iron MEMS, usually manufactured via the LIGA process, offer the possibility of larger and stronger actuators and connectors. The microstructure and mechanical properties of an electroplated material are highly dependent upon the composition of the plating bath and on the current and temperature. Similarly, the composition of a nickel–iron alloy significantly affects its characteristics. Young's modulus and strength values are listed in Tables 3.3 and 3.4 for nickel and nickel–iron respectively. The modulus of bulk nickel is around 200 GPa, and the yield strength of pure fine-grained nickel is approximately 60 MPa [ASM, 1990]. Table 3.3 shows that the modulus of nickel is generally somewhat lower and the strength considerably higher. Nickel–iron has a smaller modulus, as expected, but can be a very strong material as seen from the limited results in Table 3.4.

TABLE 3.3 Nickel

Young's Modulus (GPa)	Yield Strength (GPa)	Ultimate Strength (GPa)	Method	Comments	Ref.
202	0.40	0.78	Tension	Vibration for modulus	Mazza et al. (1996b)
~200	—	—	Ultrasonic	3–75 μm thick	Schneider and Tucker (1996)
168–182	0.1 ± 0.01	—	FE Model	Microgrippers	Basrour et al. (1997)
205	—	—	Resonance	Also fatigue	Dual et al. (1997)
68*	—	—	Torsion	*Shear modulus	Dual et al. (1997)
176 ± 30	0.32 ± 0.03	0.55	Tension	~200 μm thick	Sharpe et al. (1997e)
131–160	0.28–0.44	0.46–0.76	Tension	Varied current	Christenson et al. (1998)
231 ± 12	1.55 ± 05	2.47 ± 0.07	Tension	6 μm thick	Greek and Ericson (1998)
180 ± 12	—	—	Resonance	Film on resonator	Kahn et al. (1998)
181 ± 36	0.33 ± 0.03	0.44 ± 0.04	Tension	LIGA 3 films	Sharpe and McAleavey (1998)
158 ± 22	0.32 ± 0.02	0.52 ± 0.02	Tension	LIGA 4 films	Sharpe and McAleavey (1998)
182 ± 22	0.42 ± 0.02	0.60 ± 0.01	Tension	HI-MEMS films	Sharpe and McAleavey (1998)
153 ± 14	—	1.28 ± 0.24*	Bending	*Modulus of rupture	Stephens et al. (1998)
156 ± 9	0.44 ± 0.03	—	Tension	Current = 20 ma/cm^2	Buchheit et al. (1999)
92	0.06/0.16*	—	*Tension/ compression	Annealed	Buchheit et al. (1999)
160 ± 1	0.28/0.27*	—	*Tension/ compression	Current = 50 ma/cm^2	Buchheit et al. (1999)
146–184	—	—	Indentation	Various locations	Buchheit et al. (1999)
194	—	—	Tension	Laser speckle	Anwander et al. (2000)

TABLE 3.4 Nickel–Iron

Young's Modulus (GPa)	Yield Strength (GPa)	Ultimate Strength (GPa)	Method	Comments	Ref.
65	—	—	Fixed ends	80% Ni–20% Fe	Chung and Allen (1996)
119	0.73	1.62	Tension	50% Ni–50% Fe	Dual et al. (1997)
115	—	—	Resonance	50% Ni–50% Fe	Dual et al. (1997)
15–54*	—	—	Torsion	*Shear modulus	Dual et al. (1997)
155	—	2.26	Tension	Electroplated	Greek and Ericson (1998)
—	1.83–2.20	2.26–2.49	Tension	HI-MEMS films	Sharpe and McAleavey (1998)

The most common MEMS material, polysilicon, is also the most tested, as Table 3.5 demonstrates. The stiffness coefficients of single-crystal silicon are well established, and the modulus in different directions can vary from 125 to 180 GPa [Sato et al., 1997]. Aggregate theories predict that randomly oriented polycrystalline silicon should have a Young's modulus between 163 and 166 GPa [Guo et al., 1992; Jayaraman et al., 1999]. Most of the modulus values in Table 3.5 are near or within this range, but some vary widely, especially when a test method is first used. An estimate of what the fracture strength should be is more difficult as it depends on the flaws in the material. Even though strength is easier to measure than modulus (one needs to measure only force), there are fewer entries. This is because many of the bending, resonance, and bulge tests do not lead to failure in the specimen.

Single-crystal silicon has also been studied extensively, as Table 3.6 shows. The modulus values are measured along particular crystallographic directions, so they should not be expected to compare with the polysilicon values.

Silicon carbide holds promise for MEMS because of its expected high stiffness, strength, and chemical and temperature stability; and Sarro (2000) provides a thorough overview of its potential. Bulk silicon carbide is commonly available, but manufacturing processes for thin, free-standing films are still in development. Table 3.7 lists results from the few tests to date; note that no strength values appear.

TABLE 3.5 Polysilicon

Young's Modulus (GPa)	Fracture Strength (GPa)	Method	Comments	Ref.
160	—	Bulge	Obtains residual stress	Tabata et al. (1989)
123	—	Fixed ends	Heavily doped	Tai and Muller (1990)
190–240	—	Bulge	Various etches	Walker et al. (1990)
164–176	2.86–3.37	Tension	Varied grain size	Koskinen et al. (1993)
—	2.11–2.77	Bending	CMOS process	Biebl et al. (1995a)
147 ± 6	—	Resonance	Temperature effects	Biebl et al. (1995b)
170	—	Bending	Varied doping	Biebl and Philipsborn (1995)
—	0.57-0.77	Tension	Weibull analysis	Greek et al. (1995)
151–162	—	Bulge	Various anneals	Maier-Schneider et al. (1995)
163	—	Resonance	Temperature effects	Michalicek et al. (1995)
171–176	—	Fixed ends	Pull-in voltage	Zou et al. (1995)
149 ± 10	—	Fixed ends	Pull-in voltage	Gupta et al. (1996)
150 ± 30	—	Resonance	10 μm thick	Kahn et al. (1996)
140*	0.70	Tension	*Approximate	Read and Marshall (1996)
152–171	—	Ultrasonic	0.4 μm thick	Schneider and Tucker (1996)
176–201	—	Indentation	Different depths	Bhushan and Li (1997)
160–167	1.08–1.25	Tension	Weibull analysis	Greek and Johansson (1997)
178 ± 3	—	Fixed ends	Ph.D. thesis	Gupta (1997)
169 ± 6	1.20 ± 0.15	Tension	Poisson's ratio = 0.22 ± .01	Sharpe et al. (1997d)
174 ± 20	2.8 ± 0.5	Bending	Tested by Jones et al.	Sharpe et al. (1998c)
132	—	Tension	Tested by Chasiotis et al.	Sharpe et al. (1998c)
137 ± 5	2.7 ± 0.2	Resonance	Tested by Brown et al.	Sharpe et al. (1998c)
140 ± 14	1.3 ± 0.1	Tension	Tested by Sharpe et al.	Sharpe et al. (1998c)
172 ± 7	1.76	Tension	10 μm thick	Greek and Ericson (1998)
162 ± 4	—	Bulge	Poisson's ratio = 0.19 ± .03	Jayaraman et al. (1998)
168 ± 4	—	Resonance	0.45–0.9 μm thick	Kahn et al. (1998)
135 ± 10	—	Bending	AFM	Serre et al. (1998)
95–167	—	Indentation	Also wear tests	Sundararajan and Bhushan (1998)
167	2.0–2.7	Tension	Modulus from bulge; P-doped	Tsuchiya et al. (1998a)
163	2.0–2.8	Tension	Modulus from bulge; undoped	Tsuchiya et al. (1998a)
—	1.8–3.7	Tension	Different sizes and anneals	Tsuchiya et al. (1998b)
95/175	—	Indentation	Doped and undoped	Li and Bhushan (1998)
198	—	Bending	Capacitive device	Que et al. (1999)
166 ± 5	1.0 ± 0.1	Tension	Force-displacement	Chasiotis and Knauss (2000)
—	4.27 ± 0.61	Tension	By LaVan et al.	LaVan et al. (2000b)
—	2.85 ± 0.40	Tension	By Sharpe et al.	LaVan et al. (2000b)
—	3.23 ± 0.25	Tension	By Tsuchiya et al.	LaVan et al. (2000b)
158 ± 8	1.56 ± 0.25	Tension	Size effects	Sharpe and Jackson (2000)
159 and 169	—	Tension	Two specimens from Sharpe	Yi (pers. comm.)
—	3.2 ± 0.3	Bending	Assumed E = 160 GPa	Jones et al. (2000)
—	2.9 ± 0.5	Tension	4 μm thick	Kapels et al. (2000)
—	3.4 ± 0.5	Bending	4 μm thick	Kapels et al. (2000)

Silicon nitride commonly appears in both MEMS and in microelectronics as an insulating layer, and interest in its use as a structural material is growing. Table 3.8 lists its properties. Silicon oxide is also typically included in a MEMS or microelectronics process, but it is less likely to be used as a structural component because of its low stiffness and strength, as shown in Table 3.9.

To date, the main application of the polymer SU-8 is as a mask material for thicker electroplated metal MEMS. Its use as a structural component is possible, but the values of stiffness and strength in Table 3.10 are very low.

Fracture toughness values have been measured for polysilicon; Table 3.11 lists the results. Note that this is not the plane-strain fracture toughness that is a materials property; care is needed, as some authors list this value as KIc.

TABLE 3.6 Silicon Crystals

Young's Modulus (GPa)	Fracture Strength (GPa)	Method	Comments	Ref.
177 ± 18	2.0–4.3	Bending	⟨110⟩	Johansson et al. (1988)
188	—	Indentation		Weihs et al. (1989)
163	>3.4	Bending	⟨110⟩	Weihs et al. (1989)
122 ± 2	—	Bending	⟨110⟩	Ding et al. (1989)
125 ± 1	—	Resonance	⟨110⟩	Ding et al. (1989)
131	—	Resonance		Zhang et al. (1991)
173 ± 13	—	Bending	⟨110⟩	Osterberg et al. (1994)
147	0.26–0.82	Tension	⟨110⟩	Cunningham et al. (1995)
—	8.5–20	Torsion	Shear and normal	Saif and MacDonald (1996)
60–200	—	Indentation	Various doping	Bhushan and Li (1997)
130	—	Resonance	⟨100⟩	Dual et al. (1997)
75	—	Torsion	Shear modulus	Dual et al. (1997)
125–180	1.3–2.1	Tension	Three orientations	Sato et al. (1997)
—	9.5–26.4	Bending	Various etches	Chen et al. (1998)
—	0.7–3.0	Bending	Measured roughness	Chen et al. (1999)
142 ± 9	1.73	Tension	⟨100⟩	Greek and Ericson (1998)
165 ± 20	2–8	Bending	Fatigue tests also	Komai et al. (1998)
168	—	Indentation	⟨100⟩	Li and Bhushan (1999)
—	0.59 ± 0.02	Tension	⟨100⟩	Mazza and Dual (1999)
—	2–6	Bending	Fatigue also	Minoshima et al. (1999)
169.2 ± 3.5	0.6–1.2	Tension	Various etches	Yi and Kim (1999b)
115–191	—	Tension	Three orientations	Yi and Kim (1999c)
164.9 ± 4	—	Tension	Laser speckle	Anwander et al. (2000)
169.9	0.5–17	Bending	Various sizes	Namazu et al. (2000)

TABLE 3.7 Silicon Carbide

Young's Modulus (GPa)	Fracture Strength (GPa)	Method	Comments	Ref.
394	—	Bulge	3C–SiC	Tong and Mehregany (1992)
88 ± 10 to 242 ± 30	—	Bulge + indentation	Amorphous SiC	El Khakani et al. (1993)
694	—	Resonance	3C–SiC	Su and Wettig (1995)
100–150	—	Ultrasonic	0.2–0.3 μm thick	Schneider and Tucker (1996)
331	—	Bulge	3C–SiC; assumed	Mehregany et al. (1997)
$n = 0.25$ 196 and 273	—	Acoustic microscopy	Amorphous SiC	Cros et al. (1997)
395	—	Indentation	3C–SiC	Sundararajan and Bhushan (1998)
470 ± 10	—	Bending	3C–SiC	Serre et al. (1999)

Poisson's ratio is an important materials property when the stress state is biaxial, but only a very limited number of measurements have been made. Those are listed in the comments columns of the tables.

The question of the effect of size on the strength of MEMS materials often arises. This is because MEMS structural components can be on the same size scale as fine single-crystal "whiskers" of materials, which can have very high strengths, the premise being that they have fewer imperfections. However, there are no dramatic increases in strength because the materials still have fine grains relative to the specimen size. Tsuchiya et al. (1998) found an increase in the tensile strength of polysilicon specimens 2.0 μm thick as their length increased from 30 to 300 μm, but the gain was only 30%. Recent results show that the modulus of polysilicon does not vary with specimen size, but the strength increases from 1.21 to 1.65 GPa with decreasing specimen size [Sharpe et al., 2001]. From a practical point of view, the effect of size on strength for common MEMS structural components is not a concern.

On the other hand, Namazu et al. (2000) tested silicon crystal beams ranging in width from 0.2 to 1.04 mm, in thickness from 0.25 to 0.52 mm and in length from 6 to 9.85 mm. The beams were prepared by anisotropic etching; the smallest were tested using an atomic force microscope, and the largest with a